RESEARCH ARTICLE

Activated T Cells Break Tumor Immunosuppression by Macrophage Reeducation

Rosa Trotta[1,2], Silvia Rivis[1,2], Shikang Zhao[1,2], Marie-Pauline Orban[1,2], Sarah Trusso Cafarello[1,2], Iris Charatsidou[1,2], Joanna Pozniak[3,4], Jonas Dehairs[5], Lotte Vanheer[1,2], Carlos A. Pulido Vicuna[3,4], Veerle Boecxstaens[6], Oliver Bechter[7], Francesca M. Bosisio[8], Johannes V. Swinnen[5], Jean-Christophe Marine[3,4], and Massimiliano Mazzone[1,2,9,10]

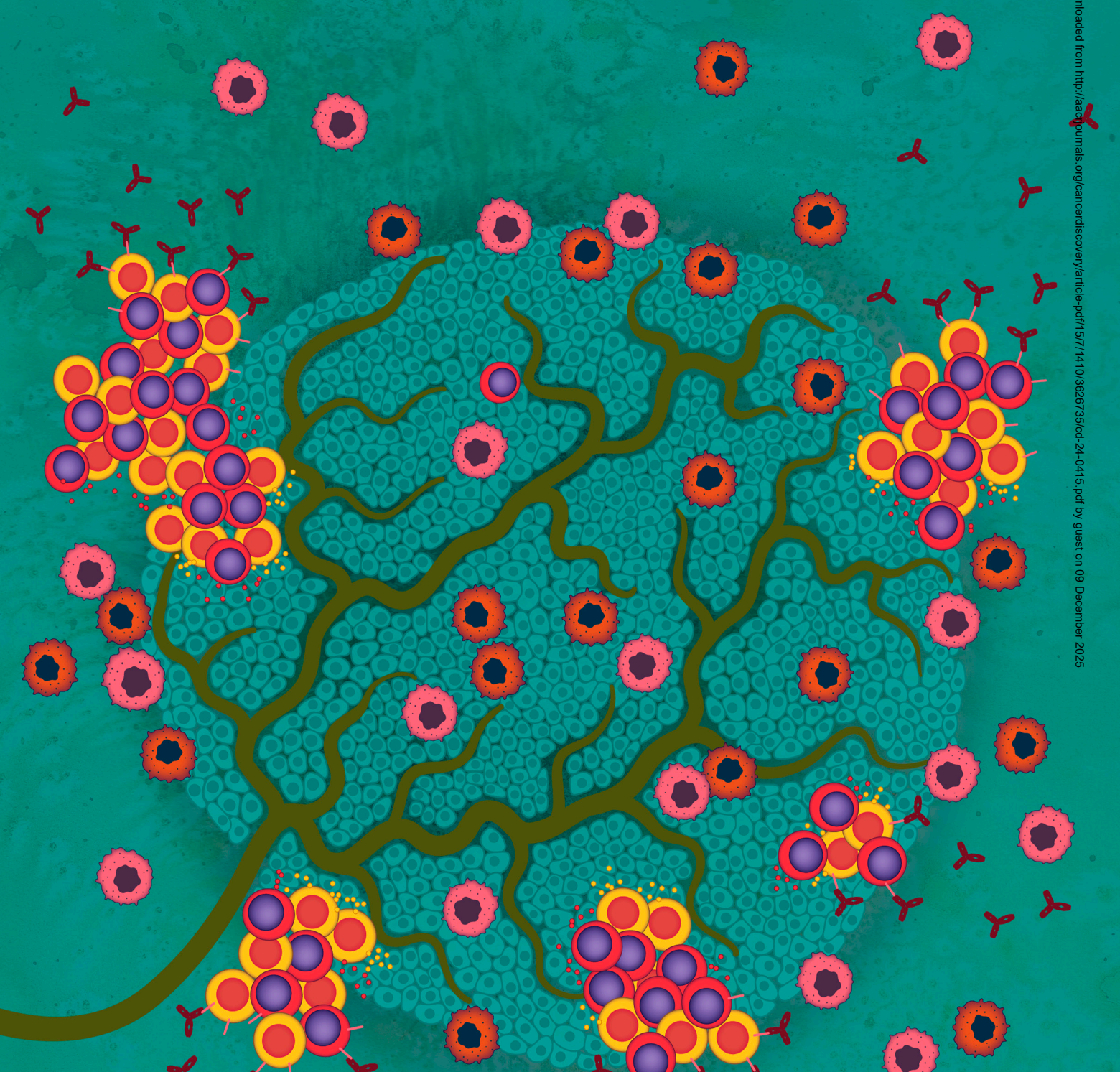

ABSTRACT In this study, we observe that in human and murine melanomas, T-cell activation abates hematopoietic prostaglandin-D2 synthase (*HPGDS*) transcription in tumor-associated macrophages (TAM) through TNFα signaling. Mechanistically, HPGDS installs a prostaglandin D_2 (PGD_2) autocrine loop in TAMs via DP1 and DP2 activation that sustains their protumoral phenotype and promotes paracrine inhibition of $CD8^+$ T cells via a PGD_2–DP1 axis. Genetic or pharmacologic HPGDS targeting induces antitumoral features in TAMs and favors $CD8^+$ T-cell recruitment, activation, and cytotoxicity, altogether sensitizing tumors to αPD1. Conversely, HPGDS overexpression in TAMs or systemic TNFα blockade sustains a protumoral environment and αPD1 resistance, preventing the downregulation of HPGDS by T cells. Congruently, patients and mice resistant to αPD1 fail to suppress HPGDS in TAMs, reinforcing the evidence that circumventing HPGDS is necessary for efficient αPD1 treatment. Overall, we disclose a mechanism whereby T-cell activation controls the innate immune system, and we suggest HPGDS/PGD_2 targeting to overcome immunotherapy resistance.

SIGNIFICANCE: In this study, we show a mechanism whereby T-cell activation controls the innate immune system and shapes the tumor microenvironment by reducing PGD_2 production in TAMs. We suggest HPGDS inhibition as a promising strategy to treat refractory tumors to current immunotherapies or to overcome acquired resistance to immune checkpoint blockade.

INTRODUCTION

Although the field of cancer immunotherapy has seen exciting therapeutic advances over the past decade, a large number of patients with solid tumors display resistance (1). Melanoma is the most aggressive form of skin cancer and the first approved tumor indication for immune checkpoint blockade (ICB) therapies (2). Currently, αPD1 alone or in combination with αCTLA4 is the first-line treatment for metastatic melanoma (3). However, 65% of patients with melanoma still do not respond to ICB (4). According to the International Agency for Research on Cancer, the annual number of melanoma cases is predicted to increase by more than 50% by 2040 (5). Therefore, additional strategies to induce antitumor immunity, alone or in combination with available immunotherapeutic drugs, are urgently needed.

Tumor-associated macrophages (TAM) are the most abundant immune cells in the tumor microenvironment (TME) and are known to dampen antitumor immunity and promote tumor growth and metastasis. Consequently, strategies that alter the TAM phenotype away from its immunosuppressive state are expected to become the next generation of immunotherapies (6, 7). However, it remains understudied how current ICB sculpts TAM functions (8, 9), therefore limiting the therapeutic options to alter their phenotype. Lately, there has been growing interest in how eicosanoids regulate antitumor immunity, cancer growth, invasion, and metastasis (8–11). Eicosanoids represent a family of inflammatory lipid mediators originating from arachidonic acid metabolism. These molecules play a key role in how immune cells interact and function. In cancer, most of the studies have been focused on prostaglandin E_2 (PGE_2; refs. 9–13). PGE_2 was primarily linked with immunosuppression, T-cell dysfunction, and resistance to ICB in multiple cancer types (14–17). However, only a few studies have investigated the role of other prostaglandins, such as prostaglandin D_2 (PGD_2), whereas the role of the enzymes involved in this pathway remains unknown. PGD_2 exerts its function by binding one of two G-protein–coupled receptors, DP1 and DP2. This lipid mediator is synthesized by the action of two types of PGD_2 synthase isoforms, lipocalin–PGD_2 synthase (LPGDS) and hematopoietic PGD_2 synthase (HPGDS). LPGDS is expressed in the central nervous system, male genitals, and heart, and it regulates numerous neurologic processes, including brain protection against ischemia (18). Instead, HPGDS expression was found in the intestine, adipose tissue, placenta, fetal liver, and nasal

[1]Laboratory of Tumor Inflammation and Angiogenesis, Center for Cancer Biology, VIB, Leuven, Belgium. [2]Laboratory of Tumor Inflammation and Angiogenesis, Center for Cancer Biology, Department of Oncology, KU Leuven, Leuven, Belgium. [3]Laboratory for Molecular Cancer Biology, Center for Cancer Biology, VIB, Leuven, Belgium. [4]Laboratory for Molecular Cancer Biology, Center for Cancer Biology, Department of Oncology, KU Leuven, Leuven, Belgium. [5]Laboratory of Lipid Metabolism and Cancer, Department of Oncology, KU Leuven, Leuven, Belgium. [6]Department of Surgical Oncology, UZ Leuven, Leuven, Belgium. [7]Department of General Medical Oncology, UZ Leuven, Leuven, Belgium. [8]Laboratory of Translational Cell & Tissue Research, Department of Pathology, UZ Leuven, Leuven, Belgium. [9]Laboratory of Immuno-Oncology and Macrophage Dynamics, IRCCS Humanitas Research Hospital, Milan, Italy. [10]Laboratory of Immuno-Oncology and Macrophage Dynamics, Department of Biomedical Sciences, Humanitas University, Milan, Italy.

S. Rivis and S. Zhao contributed equally to this article.

Corresponding Author: Massimiliano Mazzone, VIB-KU Leuven Center for Cancer Biology, Campus Gasthuisberg, Herestraat 49, Box 912, Leuven B-3000, Belgium. E-mail: massimiliano.mazzone@kuleuven.be

Cancer Discov 2025;15:1410–36

doi: 10.1158/2159-8290.CD-24-0415

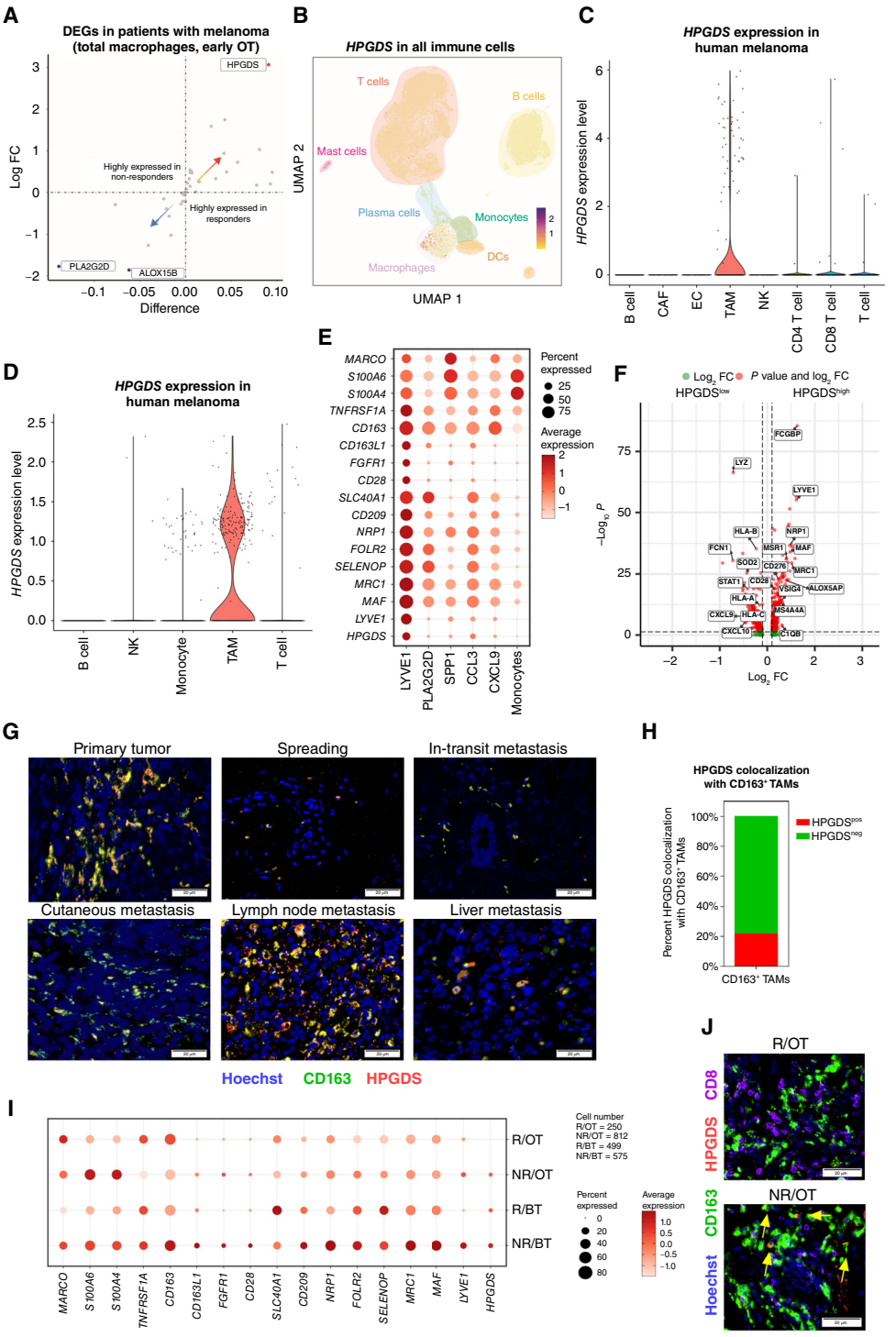

Figure 1. Identification of HPGDS in a subset of TAMs. **A,** Volcano plot extracted from an *in-house* scRNA-seq dataset, showing DEGs (out of 45 genes in the arachidonic acid metabolism) in total macrophages of NR vs. R patients with melanoma early OT with ICBs. **B,** Uniform Manifold Approximation and Projection (UMAP) representing the expression of *HPGDS* in different immune cell populations of patients with melanoma, extracted from an *in-house* scRNA-seq dataset. **C** and **D,** Violin plot from two publicly available scRNA-seq datasets of patients with melanoma, showing the expression of *HPGDS* in different tumor cell populations. **E,** *HPGDS* expression pattern in TAMs (CXCL9, CCL3, LYVE1, PLA2G2D, and SPP1) and monocytes from patients with melanoma extracted from an *in-house* scRNA-seq dataset. **F,** Volcano plot depicting DEGs between HPGDS^{high} and HPGDS^{low} macrophages in the TME of patients with melanoma. **G,** Colocalization of the macrophage-specific CD163 marker and HPGDS in primary melanomas, spreading melanomas, and melanoma metastases (i.e., in-transit metastasis, cutaneous metastasis, and lymph node or liver metastasis) of 14 patients with melanoma. **H,** Quantification of HPGDS colocalization with CD163^{+} TAMs. **I,** Dot plot of normalized expression of *HPGDS* and other protumoral genes in Rs, NRs with melanoma before treatment (BT) and early OT with ICB. **J,** Representative images of HPGDS, CD163, and CD8^{+} T-cell abundance in primary melanomas in Rs and NRs early OT with ICB. The colocalization of HPGDS with CD163 is indicated by the yellow arrowheads. *P* values were assessed by **F,** Wilcoxon test using the Seurat R package. **G** and **J,** Scale bar: 20 μm. FC, fold change.

mucosa macrophages in patients with allergic rhinitis, lung macrophages in acute respiratory distress syndrome, and adipose tissue macrophages (19). However, only a few conflicting studies have looked at how HPGDS is involved in cancer (20, 21). In this study, we used an integrative approach to unravel the functional implications of HPGDS regulation in the context of TAM biology and immunotherapy response in patients with melanoma and mouse models.

RESULTS

HPGDS Is Expressed by a Subset of TAMs in Melanoma

To identify clinically relevant genes of the arachidonic acid metabolism expressed in TAMs and regulated by ICB, we analyzed an in-house pre- and on-treatment single-cell RNA sequencing (scRNA-seq) dataset (bioRxiv 2023.12.14.571631) from patients with melanoma responding [responders (R)] or resistant [nonresponders (NR)] to ICB (23 patients were treated with αPD1, of whom six were also treated with αCTLA4) before or after the first treatment [on-treatment (OT)] with ICB. By analyzing gene expression in total TAMs, we found that of the 45 genes involved in the arachidonic acid metabolism, *HPGDS* was the only gene to be significantly higher in NRs 2 or 3 weeks after the first ICB treatment (Fig. 1A).

Looking at all the immune cell clusters within the same dataset, we found that the expression of *HPGDS* was restricted to a small cluster of mast cells and a subset of macrophages (Fig. 1B). Analysis of two other publicly available scRNA-seq datasets of patients with melanoma confirmed that *HPGDS* expression was restricted to TAMs (Fig. 1C and D; refs. 22, 23). In our *in-house* dataset, *HPGDS* was selectively expressed in a macrophage cluster characterized by the highest expression of genes such as *LYVE1*, *MRC1*, *NRP1*, *and CD163,* whereas it was barely expressed or not detected in all the other macrophage clusters (i.e., *PLA2G2D*_macrophages, *SPP1*_macrophages, *CXCL9*_macrophages, and *CCL3*_macrophages) and monocytes (Fig. 1E). This pattern of expression was consistent in all patients (Supplementary Fig. S1A). A comparison of gene expression patterns on all TAMs showed that macrophages expressing high levels of *HPGDS* fall in the protumoral signature genes (e.g., *LYVE1*, *MRC1*, *VSIG4*, *C1QB*, and *MS4A4A*; Fig. 1F; ref. 24). In line with this, in The Cancer Genome Atlas (TCGA) skin cutaneous melanoma dataset, which includes 473 patients with melanoma, we confirmed the correlation between *HPGDS* and protumoral macrophages' signature expression (Supplementary Fig. S1B). We then validated these results at the protein level by performing IHC on patient samples with primary melanomas, spreading melanomas, and melanoma metastases (i.e., in-transit metastasis, cutaneous metastasis, and lymph node or liver metastasis) of 14 patients with melanoma, showing that approximately 20% of the protumoral CD163$^+$ TAMs colocalized with HPGDS (Fig. 1G and H; Supplementary Fig. S1C; Supplementary Table S1). Notably, HPGDS expression was completely downregulated at both the RNA and protein levels in responding patients (exhibiting high CD8$^+$ T-cell expansion; ref. 25) after treatment with ICB (R/OT; Fig. 1I and J). In contrast, HPGDS remained high in resistant patients during ICB treatment (NR/OT; Fig. 1I and J). Among the 177 differentially expressed genes (DEG) in *LYVE1*_macrophages, only *HPGDS* and another gene were downregulated after αPD1 treatment in Rs (Supplementary Fig. S1D). *HPGDS* stayed low or undetectable in all the other subsets after αPD1 treatment (Supplementary Fig. S1E). Paired analysis of samples collected from the same patient before and on treatment showed also a reduction of *HPGDS* in Rs after ICB, which reached almost significance despite the small sample size ($N = 9$, $P = 0.059$; Supplementary Fig. S1F).

Consistent with the initial therapeutic scheme, we considered an independent cohort of 46 patients, all treated with αPD1 and 11 of these with αCTLA4 as well (23). Also in this case, macrophage *HPGDS* was downregulated in Rs after ICB treatment (Supplementary Fig. S1G).

Together, these observations suggest that HPGDS may serve as a marker for identifying a subset of potentially immunosuppressive macrophages in which its downregulation is a sign of efficient αPD1 treatment.

HPGDS in TAMs Promotes Immune Tolerance and a Protumoral TME

Analysis of a publicly available scRNA-seq dataset from YUMM 1.7 mouse melanomas (carrying the clinically relevant mutations *Braf*$^{V600E/+}$; *Pten*$^{-/-}$; *Cdkn2*$^{-/-}$; ref. 26) confirmed that, as in humans, *Hpgds* was mainly expressed by a cluster of *Mrc1*_TAMs and by a small cluster of mast cells (Supplementary Fig. S2A). *Hpgds* was not detected in either *Ifn*_TAMs (Fig. 2A) or monocytes (Fig. 2B). To validate the scRNA-seq data, we sorted all the different cell types composing the TME of orthotopically (intradermally) engrafted YUMM 1.7 melanomas. Among all the cell types, *Hpgds* was almost exclusively expressed in TAMs (Supplementary Fig. S2B). In line with a recent report (27), *Hpgds* was also detected in T follicular helper cells in lymph nodes; however, this expression was 80-fold lower than in TAMs (Supplementary Fig. S2C). Protein validation confirmed that HPGDS was detected in TAMs but not in other tumor compartments (i.e., CD8$^+$ T cells, CD4$^+$ T cells, and CD31$^+$ cells; Supplementary Fig. S2D) or in tissue macrophages from healthy organs (i.e., lung and liver; Supplementary Fig. S2E). *Hpgds* was the only PGD_2-producing enzyme in TAMs, whereas *Lpgds* was selectively expressed by the endothelium (Supplementary Fig. S2F). Supporting the hypothesis that tumor-derived cytokines induce HPGDS in TAMs, its expression was strongly promoted in bone marrow–derived macrophages (BMDM) cultured in tumor conditioned medium (TCM; Supplementary Fig. S2G) or after stimulation with protumoral cytokines, including IL-4, IL-6, or IL-10 (Fig. 2C). However, when removing the protumoral cytokine (e.g., IL-4) and adding a proinflammatory stimulus, such as TNFα, LPS, or LPS plus INFγ, *Hpgds* expression was downregulated (Fig. 2C). IFNγ alone did not elicit any effect (Fig. 2C). Consistently, ELISA measurements proved a higher concentration of PGD_2 in the culture medium of IL-4–polarized macrophages that decreased to control levels 24 hours after TNFα administration (Fig. 2D). *Hpgds* downmodulation in IL-4–polarized BMDMs was also driven by either the coculture with activated T cells or activated T-cell CM and restored by neutralizing TNFα (Fig. 2E; Supplementary Fig. S2H) but not, for example, by αINFγ antibodies (Supplementary Fig. S2I).

Next, we studied *in vivo* the regulation of HPGDS in macrophages upon T-cell depletion or αPD1 treatment in ICB-resistant (YUMM 1.7) versus responsive (YUMMER 1.7) melanomas (Fig. 2F and G; Supplementary Fig. S2J–S2Q; ref. 28). In the resistant YUMM 1.7 model, tumor growth (Supplementary Fig. S2J–S2M) and the abundance of HPGDS$^+$ macrophages were not affected by either CD8$^+$ T-cell depletion or αPD1 treatment (Fig. 2H and I). In contrast, in the responsive YUMMER 1.7 model, depletion of CD8$^+$ T cells (but not of CD4$^+$ T cells; Supplementary Fig. S3A–S3C) favored tumor progression (Supplementary Fig. S2N–S2Q) and accumulation of HPGDS$^+$ macrophages (Fig. 2H and I), whereas αPD1 treatment efficiently decreased both parameters (Fig. 2H and I; Supplementary Fig. S2N and S2P). Neither αCD8 nor αPD1 affected total TAMs, as demonstrated by histologic examination (Supplementary Fig. S3D). The reduction of HPGDS$^+$ TAMs upon αPD1 treatment in responsive (but not in resistant) melanomas was mediated by the effect of αPD1 on CD8$^+$ T cells because it was lost following αCD8 and αPD1 combined treatment (Supplementary Fig. S2N and S2Q). In line with the coexpression of *Hpgds* and *Mrc1*, the increase in HPGDS$^+$ macrophages was linked to increased CD206$^+$ TAMs (Fig. 2J). We also observed that the tumor vasculature was denser and more abnormal (with reduced vessel perimeter, size, and coverage) in those conditions in which HPGDS$^+$ TAMs were more abundant (Fig. 2H–M). Conversely, tumor vessels were fewer and "normalized" (29–35) when the number of HPGDS$^+$ TAMs was lower (Fig. 2H–M; Supplementary Fig. S3E and S3F).

We then attempted to prevent HPGDS downregulation by using both pharmacologic and genetic approaches. First, we treated ICB-responsive YUMMER 1.7 tumors with the TNFα trap Enbrel in combination with αPD1. Blocking TNFα with Enbrel made the tumors resistant to αPD1 (Fig. 2N; Supplementary Fig. S3G–S3I). Unlike αPD1 alone, the combination with Enbrel restored the density of HPGDS$^+$ TAMs to the same level as seen in control tumors, whereas total TAM infiltration did not change in any of the conditions tested (Fig. 2O–Q).

Following these findings, we compared immunotherapy efficiency *in vivo* in a wild-type (WT) context (Ctrl) or under constitutive *Hpgds* expression (KI) driven by the macrophage-specific promoter *CD68* (Supplementary Fig. S4A and S4B). In Ctrl mice, αPD1 efficiently inhibited YUMMER 1.7 tumor growth (Fig. 3A and B; Supplementary Fig. S4C and S4D), and this response was linked to the expansion of CD8$^+$ T cells (Fig. 3C) and the reduction of *Hpgds* in macrophages, measured at the transcript or protein level (Fig. 3D–F). Constitutive *Hpgds* expression in KI mice induced overt immunotherapy resistance (Fig. 3A and B; Supplementary Fig. S4E and S4F), with CD8$^+$ T-cell density remaining the same after αPD1 treatment and even lower than in IgG-treated Ctrl mice (Fig. 3C). Supporting the quality of our genetic approach, HPGDS in macrophages was augmented at both mRNA and protein levels within YUMMER 1.7 tumors in KI mice and did not change after αPD1 treatment (Fig. 3D–F). Total TAMs were comparable in IgG- and αPD1-treated Ctrl or KI mice (Supplementary Fig. S4G). As demonstrated by histologic examination, αPD1 response in Ctrl mice was associated with fewer but better blood vessels (bigger, more covered, and perfused; Fig. 3G–K), lower tumor hypoxia (Fig. 3L and M), and lung metastasis inhibition (Fig. 3N). Constitutive *Hpgds* expression in KI mice was sufficient to induce tumor vessel "abnormalization" and hypoxia in untreated or αPD1-treated mice (Fig. 3L and M). These data suggest a feedforward loop in which activated T cells release TNFα that downregulates HPGDS in immunosuppressive macrophages, which, in turn, lose their inhibitory capacity on T-cell activation (Fig. 3O). Overall, HPGDS downmodulation in TAMs is instrumental in promoting immunosurveillance and an antitumoral TME. Conversely, HPGDS expression shapes a protumoral TME and supports αPD1 resistance.

Hpgds Deletion in TAMs Shapes the TME toward Immunosurveillance, Vessel Normalization, and Response to Immunotherapy

We then generated *Hpgds* floxed mice that we intercrossed with the CD64:Cre line (CD64:Cre$^{Tg/W}$; *Hpgds*$^{L/L}$; *Hpgds*$^{\Delta M\phi}$ in short) so that *Hpgds* was specifically deleted in macrophages. The deletion was validated in TAMs sorted from intradermal YUMM 1.7 melanomas (Supplementary Fig. S4H)

Figure 2. HPGDS expression in macrophages is sustained byprotumoral cytokines and is downmodulated by activated T cells. **A,** Violin plot comparing *Hpgds* expression between *Ifn*$^+$ and *Mrc1*$^+$ macrophages, extracted from a publicly available scRNA-seq dataset. **B,** *Hpgds* expression assessed by qRT-PCR in monocytes (CD45$^+$, CD11b$^+$, and CD115$^+$) and TAMs (CD45$^+$, CD11b$^+$, and F4/80$^+$) from melanoma-bearing mice ($n = 3$). **C,** qRT-PCR analysis of the expression of *Hpgds* in BMDMs Ctrl or stimulated with antitumoral stimuli (i.e., IFNγ with LPS), protumoral cytokines (i.e., IL-4, IL-6, and IL-10) or with IL-4 and after IL-4 washout, with antitumoral stimuli (e.g., TNFα, IFNγ, and LPS, alone or in combination; $n = 3$). **D,** Extracellular levels of PGD_2 measured by ELISA in BMDMs Ctrl or stimulated with IL-4 or first with IL-4 and then with TNFα ($n = 3$). **E,** qRT-PCR analysis showing the regulation of *Hpgds* expression in IL-4–polarized BMDMs alone (Ctrl) or cocultured with preactivated CD8$^+$ T cells or CD8$^+$ T-cell CM with an isotype or an αTNFα blocking antibody ($n = 3$–4). **F** and **G,** Tumor growth of resistant (YUMM 1.7; **F**) vs. responsive (YUMMER 1.7; **G**) melanoma tumors treated with IgG control, αCD8 antibody, αPD1, or the combination of αCD8 and αPD1 ($n = 3$–4). **H** and **I,** Quantification (**H**) and representative images (**I**) of HPGDS$^+$ macrophages in resistant (YUMM 1.7) vs. responsive (YUMMER 1.7) melanoma tumors treated with IgG control, αCD8 antibody, αPD1, or the combination of αCD8 and αPD1 ($n = 3$–4). **J,** Quantification of CD206$^+$ immunosuppressive macrophages in resistant (YUMM 1.7) vs. responsive (YUMMER 1.7) melanoma tumors treated with IgG control, αCD8 antibody, αPD1 or the combination of αCD8 and αPD1 ($n = 3$–4). **K,** Quantification of vessel density in resistant (YUMM 1.7) vs. responsive (YUMMER 1.7) melanoma tumors treated with IgG control, αCD8 antibody, αPD1, or the combination of αCD8 and αPD1 ($n = 3$–4). **L** and **M,** Quantification (**L**) and representative images (**M**) of αSMA$^+$ pericyte blood vessel coverage of YUMM 1.7 or YUMMER 1.7 melanoma-bearing mice treated with IgG, αCD8, αPD1, or the combination of αCD8 and αPD1 ($n = 3$–4). **N,** Tumor growth of YUMMER 1.7 melanoma-bearing mice treated with IgG, αPD1, or αPD1 combined with Enbrel ($n = 8$–9). **O,** Quantification of F4/80$^+$ macrophages in YUMMER 1.7 melanoma tumors treated with IgG, αPD1, or αPD1 in combination with Enbrel. In the group treated with αPD1, three out of nine tumors regressed completely; thus, the staining was not performed ($n = 6$–9). **P** and **Q,** Quantification (**P**) and representative images (**Q**) of HPGDS$^+$ macrophages in YUMMER 1.7 melanoma tumors treated with IgG, αPD1, or αPD1 in combination with Enbrel. In the group treated with αPD1, three out of nine tumors regressed completely; thus, further analyses were not performed ($n = 6$–9). *P* values are calculated by (**A**) two-sided Wilcoxon test, (**B**) unpaired, two-tailed Student *t* test, (**C**) one-way ANOVA with Dunnett correction, and (**D**, **E**, **H**, **J**, **K**, **–L**, **O**, and **P**) one-way ANOVA with the Tukey multiple comparison test. **F**, **G** and **N,** two-way repeated measures ANOVA. Graphs show the mean ± SEM. **I**, **L** and **Q,** Scale bar: 20 μm.

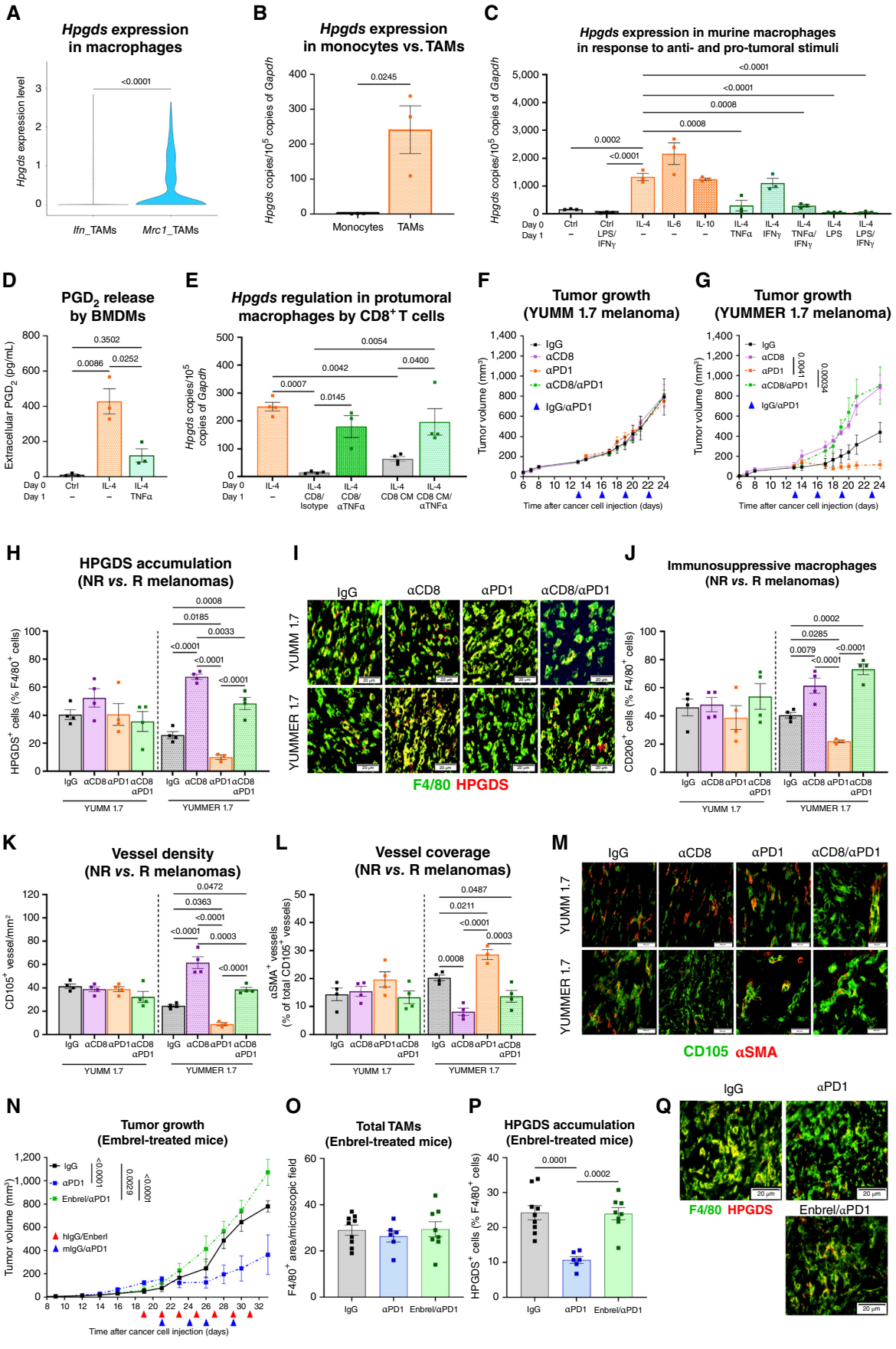

and in BMDMs isolated from *Hpgds*$^{\Delta M\phi}$ versus Ctrl mice (CD64:Cre$^{W/W}$; *Hpgds*$^{L/L}$; Ctrl in short; Supplementary Fig. S4I). Mass spectrometry analysis of tumor interstitial fluids revealed a reduction in PGD_2 but not in PGE_2 upon macrophage-specific *Hpgds* deletion (Fig. 4A; Supplementary Fig. S4J). A similar decrease was observed in PGD_2 in tumor lysates and BMDMs (Fig. 4B; Supplementary Fig. S4K).

When monitoring the growth of orthotopic YUMM1.7 melanomas, tumor volume, and weight were significantly lower (80% and 60%, respectively) in *Hpgds*$^{\Delta M\phi}$ mice compared with Ctrl littermates, with four of nine *Hpgds*$^{\Delta M\phi}$ mice displaying tumor rejection (Fig. 4C and D; Supplementary Fig. S4L and S4M). Circulating and lung disseminated cancer cells were reduced in *Hpgds*$^{\Delta M\phi}$ versus Ctrl mice (Fig. 4E–G; Supplementary Fig. S4N).

Unbiased analysis of the whole transcriptome highlighted a milder immunosuppressive and angiogenic signature of *Hpgds* knockout (KO) versus Ctrl TAMs directly sorted from YUMM 1.7 tumors (Supplementary Fig. S4O) with independent confirmation by qRT-PCR of some of the regulated genes, *e.g.*, *Cxcl9*, *Cxcl10*, *Cxcl11*, *Cd80*, *Fgf2*, and *Hgf* (Supplementary Fig. S4P–S4U). FACS and histologic analyses confirmed that tumors in *Hpgds*$^{\Delta M\phi}$ mice had decreased CD206$^+$, CD204$^+$, and MHC-II^{low} macrophages but were enriched for CD11c, CD80, CD86, and MH-CII (Fig. 4H–J), although the total number of TAMs was not altered (Supplementary Fig. S5A and S5B). CD8$^+$ T-cell infiltration was also increased with higher expression of activation/effector markers such as CD69, IFNγ, and granzyme B (GZMB; Fig. 4K and L). In contrast, conventional dendritic cells (cDC), neutrophils, and CD4$^+$ T cells were unaffected (Supplementary Fig. S5C–S5G). Additionally, following *Hpgds* deletion in TAMs, tumor blood vessels were fewer but larger with improved pericyte coverage and perfusion (Fig. 4M–U).

To assess the contribution of CD8$^+$ T cells in the inhibition of tumor growth and metastatic dissemination, we administered CD8-depleting antibodies (Supplementary Fig. S5H). This treatment restored YUMM 1.7 tumor growth in *Hpgds*$^{\Delta M\phi}$ mice to the same level as in Ctrl littermates (Fig. 4V and W; Supplementary Fig. S5I–S5L). In contrast, CD8$^+$ T-cell depletion did not affect the abundance of CD80$^+$ TAMs, tumor vessel normalization, and lung colonization inhibition in *Hpgds*$^{\Delta M\phi}$ mice (Fig. 4X and Y; Supplementary Fig. S5M–S5O). Therefore, CD8$^+$ T cells are required to restrain tumor growth in *Hpgds*$^{\Delta M\phi}$ mice, but the effect on tumor vessels and cancer cell dissemination can be ascribed to macrophage reeducation.

Finally, Ctrl and *Hpgds*$^{\Delta M\phi}$ mice were orthotopically injected with YUMM 1.7 melanoma cancer cells and treated with αPD1 when the average tumor size of both groups was 150 mm^3 (Fig. 5A and B). Although Ctrl mice displayed resistance to αPD1, *Hpgds* deletion in macrophages sensitized tumors to αPD1 and inhibited tumor relapse (Fig. 5A and B; Supplementary Fig. S5P–S5S).

To further validate our findings, we modified hematopoietic progenitors from donor mice by using an inducible macrophage-specific CRISPR/Cas9 system, generating fully reconstituted WT (WT → WT) and macrophage-specific *Hpgds* KO (*Hpgds* KO → WT) chimeras (Supplementary Fig. S6A and S6B). Then, we intradermally injected YUMM 1.7 melanoma cancer cells into WT → WT or *Hpgds* KO → WT mice. *Hpgds* genetic ablation in TAMs was confirmed at the protein level by histologic examination and Western blot (WB; Supplementary Fig. S6C and S6D). Our results confirmed reduced tumor growth (Supplementary Fig. S6E–S6G) and weight (Supplementary Fig. S6H and S6I) in Hpgds KO → WT mice. Although Hpgds deletion did not influence overall TAM infiltration (Supplementary Fig. S6J), it did promote a shift from protumoral to antitumoral markers (Supplementary Fig. S6K–S6N) and an increase in CD8$^+$ T cells (Supplementary Fig. S6O and S6P). These cells were relocalized into the tumor core (Supplementary Fig. S6Q and S6R) and displayed increased IFNγ and GZMB (Supplementary Fig. S6S).

Taken together, these data suggest that TME editing resulting from HPGDS inhibition in TAMs halts cancer growth and dissemination, sensitizing the tumors to αPD1.

Direct and Indirect Effects of HPGDS/PGD_2 Signaling Inhibition

The downstream effect of PGD_2 is mediated by the activation of two G-protein–coupled receptors, DP1 (encoded by the *PTGDR1* gene) and DP2 (encoded by the *PTGDR2* gene). Expression analysis in YUMM 1.7 melanoma tumors highlighted that, among the cells tested, *Ptgdr1* and *Ptgdr2* were higher in CD8$^+$ T cells, CD4$^+$ T cells, macrophages, and neutrophils but low or undetectable in endothelial cells (EC) and cancer cells (Supplementary Fig. S7A and S7B). Therefore, we analyzed the effect of PGD_2 on CD8$^+$ T cells and macrophages but not on CD4$^+$ T cells and neutrophils, given their unchanged chart in *Hpgds*$^{\Delta M\phi}$ mice.

It has been shown that PGD_2 antagonism confers proinflammatory features to macrophages (36). Based on our findings in TAMs and the persistence of tumor vasculature

Figure 3. *Hpgds* overexpression in macrophages promotes tumor progression and confers ICB resistance. **A** and **B,** Tumor growth and tumor weight of YUMMER 1.7 melanoma-bearing Ctrl or *Hpgds* KI mice overexpressing *Hpgds* selectively in TAMs, treated with IgG or with αPD1 ($n = 5$–6). **C,** Quantification of CD8$^+$ T cells in Ctrl and *Hpgds* KI mice treated with IgG or with αPD1 ($n = 5$–6). **D–F,** Quantification by qRT-PCR (**D**) of *Hpgds* in macrophages or histology of HPGDS$^+$ macrophages (**E**) and representative tumor section images (**F**) from YUMMER 1.7 melanoma-bearing Ctrl and *Hpgds* KI mice treated with IgG or with αPD1 ($n = 5$–6). **G** and **H,** Quantification of CD105$^+$ vessel (**G**), density (**G**), and size (**H**) in Ctrl and *Hpgds* KI mice treated with IgG or with αPD1 ($n = 5$–6). **I,** Quantification of αSMA$^+$ pericyte blood vessel coverage from YUMMER 1.7 melanoma-bearing Ctrl and *Hpgds* KI mice treated with IgG or with αPD1 ($n = 5$–6). **J** and **K,** Quantification (**J**) and representative images (**K**) of Lectin-FITC$^+$ perfused vessels in Ctrl and *Hpgds* KI mice treated with IgG or with αPD1 ($n = 5$–6). **L** and **M,** Quantification (**L**) and representative images (**M**) of the hypoxic area (PIMO$^+$) in Ctrl and *Hpgds* KI mice treated with IgG or with αPD1 ($n = 5$–6). **N,** Number of lung metastasis in *Hpgds* KI mice treated with IgG or with αPD1 ($n = 5$–6). **O,** Representative scheme showing the interaction between TNFα secreted by cytotoxic CD8$^+$ T cells upon activation and HPGDS expression in macrophages in responsive and resistant patients. *P* values are calculated by (**A**) two-way repeated-measure ANOVA, (**B**, **C**, **E**, **G–J**, **L** and **N**) one-way ANOVA with the Tukey multiple comparison test, and (**D**) multiple unpaired Student *t* test. Graphs show the mean ± SEM. **F**, **K**, and **M,** Scale bar: 20 μm. **O,** Created with BioRender.com. Trotta, R. (2025) (https://BioRender.com/y35l375).

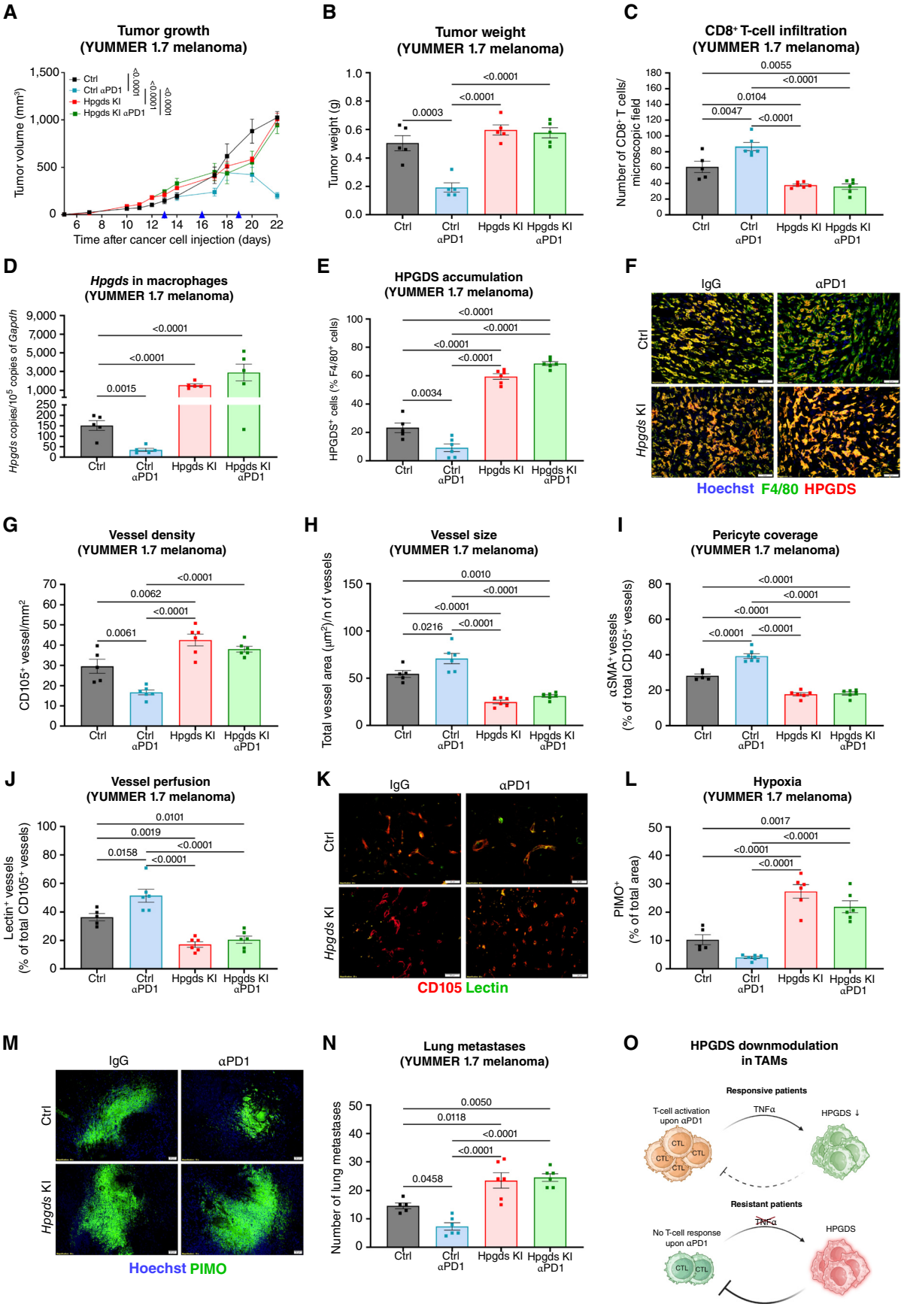

normalization in *Hpgds*$^{\Delta M\phi}$ mice following CD8$^+$ T-cell depletion, we hypothesized that PGD_2 released by HPGDS$^+$ TAMs might influence macrophage behavior, which could subsequently promote their abnormalization. In line with this, IL-4–polarized *Hpgds*$^{\Delta M\phi}$ BMDMs displayed lower levels of anti-inflammatory and angiogenic factors and higher levels of proinflammatory and vessel-stabilizing factors (Supplementary Fig. S7C). As assessed by qRT-PCR, PGD2 supplementation for 24 hours to BMDMs downregulated *Cxcl10* expression and upregulated *Mrc1*$^+$/*Cd206* levels (Fig. 5C and D). In this setting, PGD_2 stimulation did not affect *Hpgds* expression (Supplementary Fig. S7D). Functional evaluation of macrophage polarity showed that CD8$^+$ T cells migrated more toward *Hpgds*$^{\Delta M\phi}$ BMDMs than toward their control BMDMs (Fig. 5E). In contrast, prestimulation of macrophages with PGD_2 (thoroughly washed out before coculture) impaired CD8$^+$ T-cell migration (Fig. 5E). Next, to investigate the functional implication of *Hpgds*$^{\Delta M\phi}$ BMDMs in promoting vessel normalization, we conducted a 3D spheroid sprouting assay in a type I collagen gel. Coculturing *Hpgds*$^{\Delta M\phi}$ BMDMs with ECs decreased the number and the length of sprouts formed by the spheroids (Fig. 5F; Supplementary Fig. S7E). A more angiostatic phenotype of *Hpgds*$^{\Delta M\phi}$ BMDMs was further proven *in vitro* by the impaired capacity of BMDM-derived CM to modulate EC migration through a transwell filter. Endothelial migration was rescued by adding fibroblast growth factor 2 (FGF2) or hepatocyte growth factor (HGF) to the CM (Supplementary Fig. S7F). A similar rescue was achieved when human umbilical vein ECs (HUVEC) were preincubated with a BMDM CM containing a CXCR3 inhibitor in the CM and then stimulated with VEGF (Fig. 5G; Supplementary Fig. S7G). These results suggest that the negative and positive modulation of these pathways by *Hpgds* KO macrophages might contribute to the control of EC behavior. Finally, YUMM 1.7 cell migration toward *Hpgds*$^{\Delta M\phi}$ BMDMs was also impaired (Fig. 5H). Notably, PGD_2 stimulation of EC spheroids or YUMM 1.7 melanoma cancer cells did not *per se* affect their sprouting (Supplementary Fig. S7H–S7J) or migration (Supplementary Fig. S7K). These data suggest an autocrine role of HPGDS-mediated PGD_2 production on macrophage polarity but do not exclude a direct effect of PGD_2 on CD8$^+$ T cells. Therefore, we supplied the culture medium of preactivated CD8$^+$ T cells with PGD_2 and restimulated them with PMA/ionomycin. This resulted in reduced TNFα, IFNγ, and GZMB production (Fig. 5I–K) as well as diminished levels of the activation marker CD69 (Fig. 5L) and checkpoint PD1 (Fig. 5M). Functionally, ovalbumin (OVA)-specific activated OT-I T cells, stimulated with PGD_2 and primed with OVA-expressing YUMM 1.7 cells, displayed impaired proliferative capacity and cancer cell–killing (Fig. 5N; Supplementary Fig. S7L and S7M). In line with the different CD8$^+$ T-cell localization within the tumor in *Hpgds*$^{\Delta M\phi}$ mice, PGD_2 strongly inhibited CXCL10-induced migration of activated T cells (Fig. 5O). Thus, PGD_2 can affect CD8$^+$ T cells directly and indirectly through a macrophage switch.

Given that PGD_2 exerts its functions through DP1 and DP2, we sought to assess *in vivo* the extent to which these two receptors contribute to TAM reprogramming. To this end, we used the CRISPR/Cas9 technology to inhibit DP1 or DP2 in macrophages (Supplementary Fig. S8A). *Ptgdr1* or *Ptgdr2* targeting was confirmed in BMDMs obtained from the same mice at the RNA level (Supplementary Fig. S8B). When implanting YUMM 1.7 melanoma cancer cells in immune-reconstituted mice, we observed reduced tumor growth and weight upon genetic targeting of either *Ptgdr1* or *Ptgdr2* in macrophages (Fig. 5P and Q). Combined targeting of *Ptgdr1* and *Ptgdr2* in macrophages was not additive (Fig. 5P and Q; Supplementary Fig. S8C–S8F), strengthening *in vivo* the evidence that DP1 or DP2 inhibition in macrophages is *per se* sufficient to elicit a pharmacologic effect (37), possibly because of a molecular crosstalk of these two receptors. In these tumors, proficient for macrophage HPGDS and thus for PGD_2 synthesis, although the number of total TAMs was unchanged (Supplementary Fig. S8G), they had higher CD80 and lower CD206 expression (Fig. 5R), and blood vessels were fewer and better covered (Fig. 5S and T). T-cell recruitment at the tumor core was unaffected (Supplementary Fig. S8H). Targeting macrophage *Ptgdr1* or *Ptgdr2* in *Hpgds*$^{\Delta M\phi}$ mice (Supplementary Fig. S8A) did not result in any additional effects (Supplementary Fig. S8I–S8M). Thus, an autocrine effect of PGD_2 on HPGDS-expressing macrophages, requiring both DP1 and DP2, sustains their

Figure 4. *Hpgds* deletion in TAMs reshapes the TME and inhibits tumor growth. **A,** Extracellular levels of PGD_2 measured by LC/MS in the interstitial fluid of YUMM 1.7 melanoma tumors from Ctrl and *Hpgds*$^{\Delta M\phi}$ mice ($n = 4$–5). **B,** Intratumoral concentration of PGD_2 measured by LC/MS in Ctrl and *Hpgds*$^{\Delta M\phi}$ mice ($n = 3$). **C** and **D,** Tumor growth (**C**) and tumor weight (**D**) of YUMM 1.7 CD90.1$^+$ melanoma-bearing mice implanted in Ctrl or *Hpgds*$^{\Delta M\phi}$ mice ($n = 9$–11). For the analyses from **H–U**, 4 of 10 tumors in *Hpgds*$^{\Delta M\phi}$ mice were not included due to their total regression. FACS and immunofluorescence (IF) were performed by processing the same number of tumors in both groups. **E,** FACS analysis of the percentage of CD90.1$^+$ cells (out of viable) in the blood collected from Ctrl and *Hpgds*$^{\Delta M\phi}$ YUMM 1.7 melanoma-bearing mice ($n = 3$). **F,** Quantification of CD90.1$^+$ area out of Hoechst$^+$ area per lung cross-section from Ctrl and *Hpgds*$^{\Delta M\phi}$ YUMM 1.7 melanoma-bearing mice ($n = 4$). **G,** qRT-PCR analysis of *Cd90.1* expression in lungs from Ctrl or *Hpgds*$^{\Delta M\phi}$ YUMM 1.7 melanoma-bearing mice ($n = 5$). **H** and **I,** FACS analysis for MHC-II^{high}, CD11c$^+$, and CD86$^+$ (**H**) or MHC-II^{low}, CD206$^+$, and CD204$^+$ (**I**) TAMs from YUMM 1.7 melanoma-bearing Ctrl or *Hpgds*$^{\Delta M\phi}$ mice ($n = 4$). **J,** Quantification from Ctrl and *Hpgds*$^{\Delta M\phi}$ mice of melanoma sections costained for F4/80 and CD80 or CD206 ($n = 5$). **K,** FACS analysis for CD8$^+$ T-cell percentages in melanoma tumors from Ctrl and *Hpgds*$^{\Delta M\phi}$ mice ($n = 4$). **L,** Flow cytometric quantification of activated CD8$^+$ T cells (% of CD69$^+$, IFNγ$^+$, and GZMB$^+$ out of CD8$^+$ T cells) in melanoma tumors from Ctrl and *Hpgds*$^{\Delta M\phi}$ mice ($n = 5$). **M–O,** Quantification of CD105$^+$ vessel density (**M**), perimeter (**N**), and size (**O**) in melanoma tumors from Ctrl and *Hpgds*$^{\Delta M\phi}$ mice ($n = 5$). **P,** Representative images of CD105$^+$ vessels in melanoma tumors from Ctrl and *Hpgds*$^{\Delta M\phi}$ mice ($n = 5$). **Q,** Quantification of αSMA$^+$ pericyte blood vessel coverage in melanoma tumors from Ctrl and *Hpgds*$^{\Delta M\phi}$ mice ($n = 5$). **R** and **S,** Quantification (**R**) and representative images (**S**) of Lectin-FITC$^+$ perfused vessels in melanoma tumors from Ctrl and *Hpgds*$^{\Delta M\phi}$ mice ($n = 5$). **T** and **U,** Quantification (**T**) and representative images (**U**) of the hypoxic area (PIMO$^+$) in YUMM 1.7 melanoma of Ctrl and *Hpgds*$^{\Delta M\phi}$ mice ($n = 4$). **V** and **W,** Tumor growth (**V**) and tumor weight (**W**) of YUMM 1.7 CD90.1$^+$ melanoma tumors injected in Ctrl or *Hpgds*$^{\Delta M\phi}$ mice treated with IgG control or a CD8-depleting antibody ($n = 5$–6). **X,** Quantification of YUMM 1.7 melanoma sections stained for F4/80 and CD80 from Ctrl and *Hpgds*$^{\Delta M\phi}$ tumor-bearing mice treated with IgG or αCD8 ($n = 5$). **Y,** qRT-PCR analysis for *Cd90.1* in lungs collected from Ctrl and *Hpgds*$^{\Delta M\phi}$ melanoma-bearing mice treated with IgG or αCD8 antibody ($n = 3$–4). *P* values were assessed by (**A**, **B**, **D–G**, **K**, **M–O**, **Q**, **R**, and **T**) unpaired, two-tailed Student *t* test; (**C** and **V**) two-way repeated-measure ANOVA; (**H–J** and **L**) multiple unpaired Student *t* test; and (**W–Y**) two-way ANOVA with the Tukey multiple comparison test. Graphs show the mean ± SEM. Scale bar: **P** and **S**, 20 μm; **U**, 50 μm.

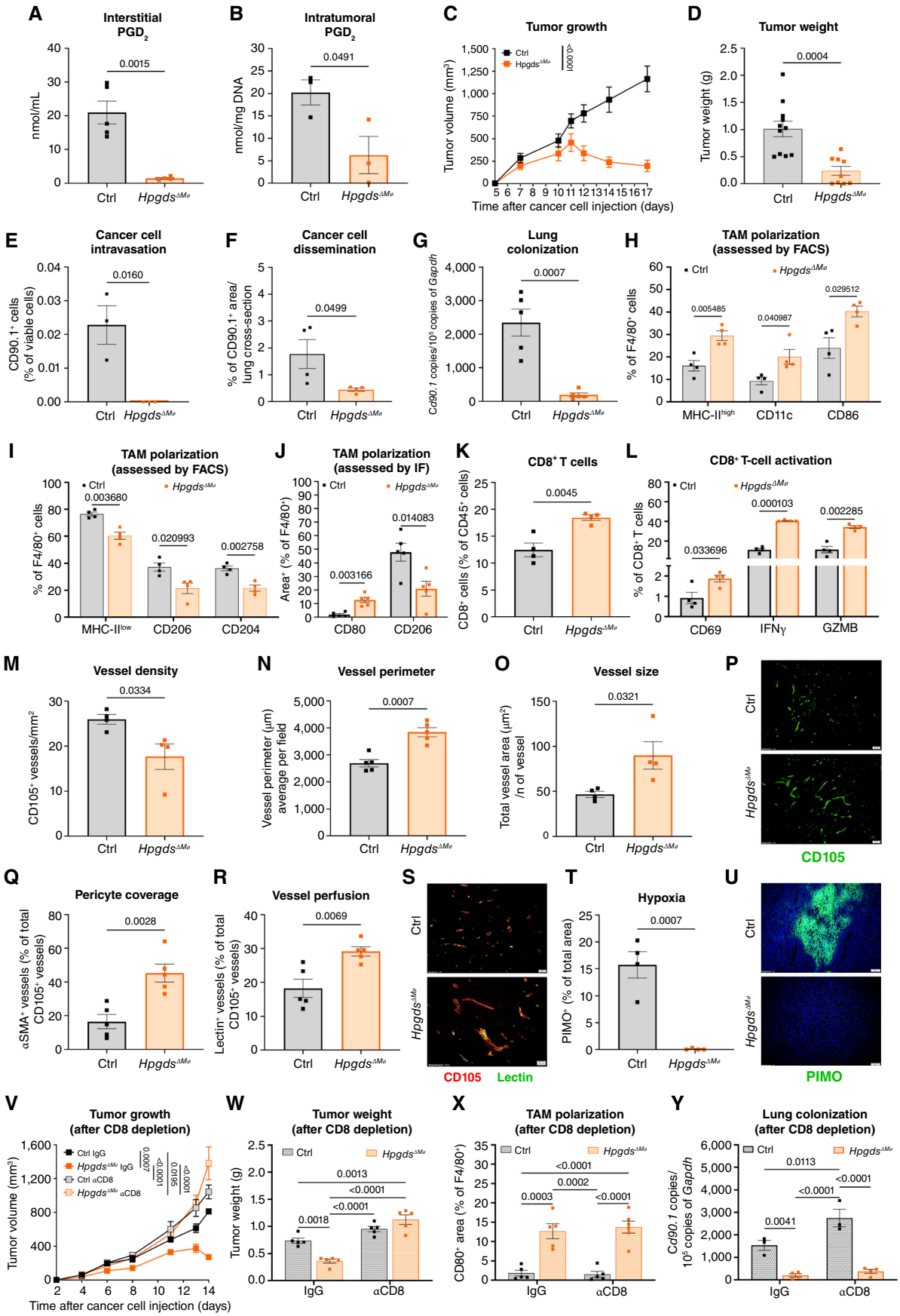

protumoral features. Interfering with this loop promotes macrophage reeducation that, in turn, affects cancer cell behavior and blood vessels in a PGD_2-independent manner. Considering the direct effect of PGD_2 on $CD8^+$ T cells, we targeted *in vivo* DP1 and DP2 in these cells by using a similar CRISPR-Cas9 strategy (Supplementary Fig. S8N and S8O). Targeting DP1, but not DP2, in $CD8^+$ T cells decreased tumor growth and weight of YUMM 1.7 melanomas (Fig. 5U and V; Supplementary Fig. S8P–S8R). In this case, TAMs and blood vessels were unchanged (Fig. 5W and X; Supplementary Fig. S8S and S8T), but $CD8^+$ T-cell infiltration at the tumor core was more pronounced (Fig. 5Y). Thus, besides other functions proven *in vitro*, PGD_2 promotes $CD8^+$ T-cell exclusion through a paracrine PGD_2/DP1 axis.

Pharmacologic HPGDS Inhibition Reshapes the TME and Blocks Tumor Growth

To translate our genetic results in a clinically relevant setting, we used the HPGDS inhibitor HQL-79 (38) in YUMM 1.7 melanoma-bearing mice. Systemic administration of HQL-79 (15 mg/kg twice daily) recapitulated the antitumor phenotype observed in $Hpgds^{\Delta M\phi}$ mice (Fig. 6A–C; Supplementary Fig. S9A and S9B), achieving 78% of tumor growth inhibition with one of six mice undergoing total tumor rejection (Supplementary Fig. S9B). The impairment in tumor growth was accompanied by a shift in TAMs toward antitumoral markers (Fig. 6D–F) and robust infiltration of $CD8^+$ T cells (Supplementary Fig. S9C–S9E). Like macrophage-specific *Hpgds* deletion, HQL-79 strongly affected the tumor vasculature by decreasing vessel density and size and by improving pericyte coverage and perfusion (Supplementary Fig. S9F–S9L), together with reduced hypoxia (Supplementary Fig. S9M and S9N), cancer cell intravasation into the bloodstream (Fig. 6G), and lung colonization (Fig. 6H). Selectivity of HQL-79 for the target was proven by intercrossing *Hpgds* floxed mice with CD64:Cre-ERT2 mice (CD64:Cre-ERT2; $Hpgds^{L/L}$; $Hpgds^{\Delta M\phi\text{-}ERT2}$ in short), in which *Hpgds* was deleted in TAMs upon intraperitoneal tamoxifen injection (Supplementary Fig. S9O). The effect of systemic inhibition and acute deletion in macrophages was comparable, with no additional effect of the inhibitor in $Hpgds^{\Delta M\phi\text{-}ERT2}$ mice (Fig. 6I and J; Supplementary Fig. S9P–S9S), a proof of compound specificity and of a major role of HPGDS in macrophages.

HQL-79 was also tested in orthotopic $NRAS^{Q61K}$; $Ink4a^{-/-}$ melanomas, resulting in 80% tumor growth inhibition with two of six mice undergoing total tumor rejection (Fig. 6K–M; Supplementary Fig. S10A and S10B).

A second HPGDS inhibitor, Cmpd1y (39), showed a dose-response effect on tumor inhibition with the highest efficacy at 3 mg/kg twice daily, i.e., 55% of tumor growth and weight inhibition (Fig. 6N and O; Supplementary Fig. S10C–S10G). A less potent HPGDS inhibitor, TAS-205 (40), also showed a robust therapeutic effect at 30 mg/kg twice daily (Fig. 6P and Q; Supplementary Fig. S10H and S10I).

Together, these data prove that pharmacologic inhibition of HPGDS could provide a promising therapeutic option against melanoma.

Further Validation of Pharmacologic HPGDS Inhibition in Clinically Relevant Mouse Models and Human Settings

Finally, we took advantage of a spontaneous $Braf^{V600E;}$ $Pten^{-/-}$ melanoma model (41), induced by the administration of 4-hydroxytamoxifen (4-HT) on the skin of these genetically engineered mice, and treated the mice with HQL-79, αPD1, or HQL-79 plus αPD1. Here, neither HPGDS inhibition by HQL-79 nor αPD1 alone affected tumor progression; however, their combination was greatly effective (Fig. 7A–C; Supplementary Fig. S11A–S11D). Albeit macrophages were acquiring immunostimulatory markers following each treatment alone or their combination (Fig. 7D), flow cytometry analysis revealed a trend toward increased infiltration of $CD8^+$ T cells in the monotherapies but overt $CD8^+$ T-cell expansion upon treatment combination (Supplementary Fig. S11E).

Figure 5. Synergism of *Hpgds* deletion with ICB and contribution of PGD_2 signaling to TAM reeducation and $CD8^+$ T-cell biology. **A** and **B,** Tumor growth (**A**) and tumor weight (**B**) from Ctrl and $Hpgds^{\Delta M\phi}$ tumor-bearing mice treated with IgG or αPD1 when the average tumor of the group was 150 mm^3. Tumors in 2 of 13 $Hpgds^{\Delta M\phi}$ mice that did not reach 150 mm^3 were not included in the experiment. **C,** qRT-PCR analysis for *Cxcl10* in IL-4–polarized Ctrl or $Hpgds^{\Delta M\phi}$ BMDMs treated or not with 1 μmol/L PGD_2 for 24 hours ($n = 4$). **D,** qRT-PCR analysis for *Cd206* in IL-4–polarized Ctrl or $Hpgds^{\Delta M\phi}$ BMDMs treated or not with 1 μmol/L PGD_2 for 24 hours ($n = 4$). **E,** Migration through 5-μm-pore polycarbonate membranes of $CD8^+$ T cells in the presence of IL-4–polarized Ctrl or $Hpgds^{\Delta M\phi}$ BMDMs pretreated or not with 1 μmol/L PGD_2 for 24 hours ($n = 3$). **F,** Quantification of the total sprout length of HUVEC spheroids embedded in collagen I in coculture with Ctrl or $Hpgds^{\Delta M\phi}$ BMDMs and supplemented with 1 μmol/L PGD_2, 50 ng/mL VEGF, or the combination of both ($n = 4$). **G,** HUVEC migration assay (through 8-μm-pore polycarbonate membranes) in which the top chamber was seeded with HUVECs pretreated for 2 hours with Ctrl or $Hpgds^{\Delta M\phi}$ macrophage CM with or without the CXCR3 inhibitor AMG 487 (500 nmol/L); 10 ng/mL VEGF were then placed in the bottom chamber. HUVEC medium without or with VEGF were used as negative and positive controls, respectively. **H,** YUMM 1.7 melanoma cancer cell migration (through 8-μm-pore polycarbonate membranes) in the presence of Ctrl or $Hpgds^{\Delta M\phi}$ BMDMs in the lower chamber ($n = 3$). **I–K,** FACS analysis of TNFα (**I**), IFNγ (**J**), and GZMB (**K**) production in activated $CD8^+$ T cells pretreated for 4 hours with 1 μmol/L PGD_2 ($n = 3$). **L** and **M,** FACS analysis of $CD69^+$ (**L**) and $PD1^+$ (**M**) activated $CD8^+$ T cells pretreated for 4 hours with 1 μmol/L PGD_2 ($n = 3$). **N,** Flow cytometric quantification of dividing (CellTrace VioletCTV) OT-I $CD8^+$ T cells prestimulated for 4 hours with 1 μmol/L PGD_2 and cocultured for 24 hours with OVA-expressing YUMM 1.7 in a ratio 2:1 ($n = 6$). **O,** Migration through 5-μm-pore polycarbonate membranes of activated $CD8^+$ T cells (prestimulated for 4 hours with 1 μmol/L PGD_2) toward medium, 50 ng/mL CXCL10, 1 μmol/L PGD_2, or the combination of both ($n = 5$). **P** and **Q,** Tumor growth (**P**) and weight (**Q**) of YUMM 1.7 melanoma tumors in nontargeting control (NT), *Ptgdr1*, *Ptgdr2,* and *Ptgdr1 Ptgdr2* KO macrophage chimeras ($n = 8$–14). **R,** Histologic quantification of CD80 or CD206 macrophages ($F4/80^+$) in melanoma from NT and *Ptgdr1 Ptgdr2* (dualKO) macrophage chimeras ($n = 8$–14). **S** and **T,** Histologic quantification of $CD105^+$ vessel density (**S**) and αSMA pericyte coverage (**T**) in melanoma tumors from NT and dualKO macrophage chimeras ($n = 8$–14). **U** and **V,** YUMM 1.7 melanoma tumor growth (**U**) and tumor weight (**V**) in chimeric mice NT, *Ptgdr1,* and *Ptgdr2* KO in $CD8^+$ T cells ($n = 7$–9). **W,** Histologic quantification of CD80 or CD206 macrophages ($F4/80^+$) in YUMM 1.7 melanoma-bearing mice from NT and *Ptgdr1* KO $CD8^+$ T-cell chimeras ($n = 7$–9). **X,** Quantification of αSMA pericyte coverage in YUMM 1.7 melanoma-bearing mice from NT and *Ptgdr1* KO $CD8^+$ T-cell chimeras ($n = 7$–9). **Y,** Histologic quantification of $CD8^+$ T cells in YUMM 1.7 melanoma-bearing mice from NT and *Ptgdr1* KO $CD8^+$ T-cell chimeras ($n = 7$–9). *P* values are assessed by (**A**, **P**, and **U**) two-way repeated measures ANOVA, (**B–E**) two-way ANOVA with Tukey multiple comparison test, (**F** and **G**) two-way ANOVA with Tukey multiple comparison test, (**H–N**, **S**, **T**, and **X**) unpaired, two-tailed Student *t* test, (**O**, **Q**, and **V**) one-way ANOVA with Tukey multiple comparison test, (**R** and **W**) multiple unpaired Student *t* test, and (**Y**), multiple paired Student *t* test. Graphs show the mean ± SEM. **P–T,** Data show a pool of two independent experiments. Nr, number.

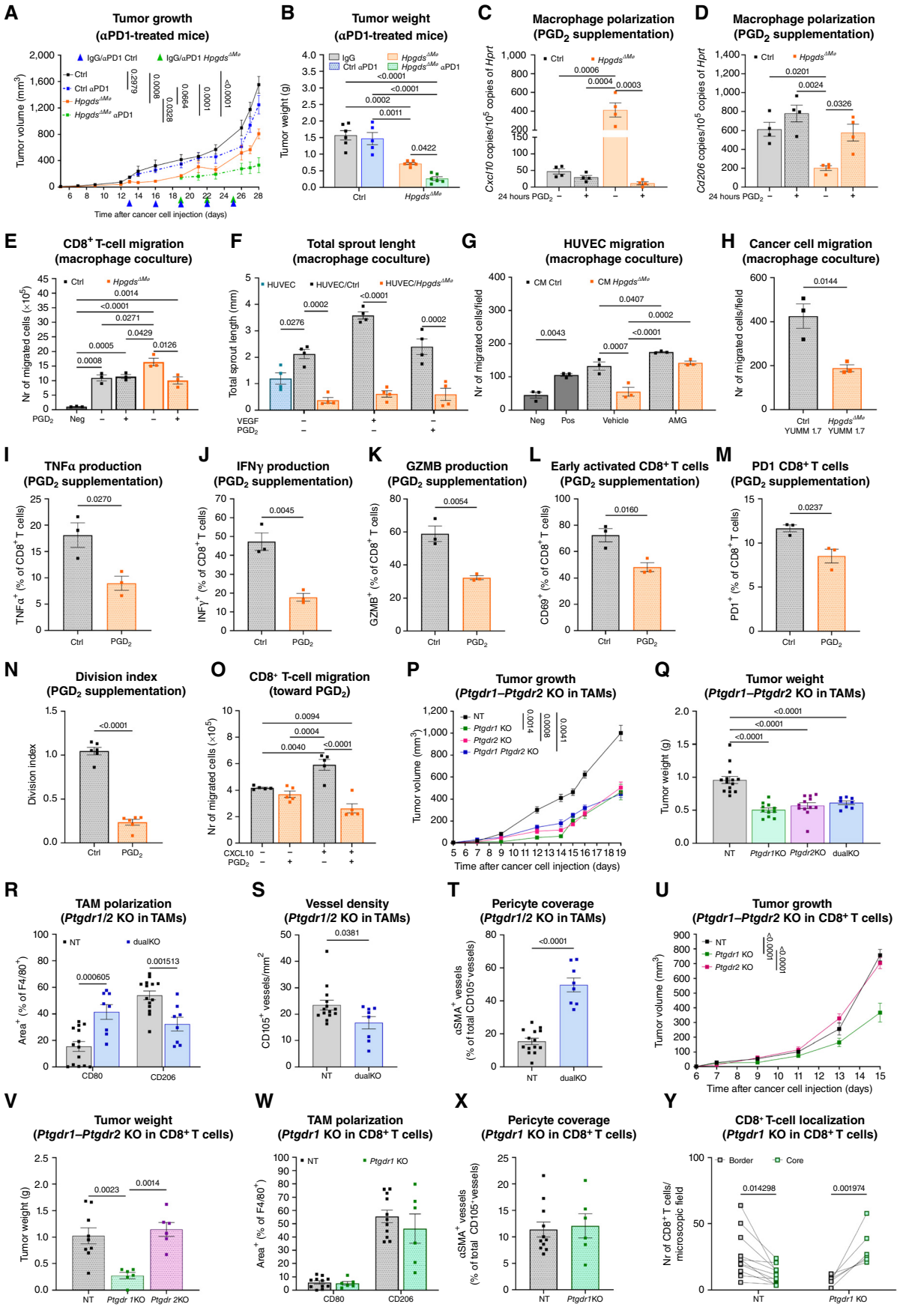

Notably, HQL-79 led to higher PD1 expression in CD8$^+$ T cells (Fig. 7E) with their relocalization from the margin to the tumor core (Fig. 7F). The recruitment of PD1$^+$ CD8$^+$ T cells to the core of the tumor upon HPGDS inhibition can explain the recovery and expansion of CD8$^+$ T cells in response to combined αPD1 treatment. Lastly, we extended our findings to pancreatic ductal adenocarcinoma (PDAC). This tumor type was selected due to the higher expression of HPGDS in the malignant tissue compared with the healthy counterpart (Supplementary Fig. S11F) and its colocalization with macrophage markers only in both murine and human tumors (Supplementary Fig. S11G). In mice with orthotopic KPC tumors (carrying the two most common mutations found in patients with PDAC, i.e., *KRAS* and *TP53*), αPD1 was ineffective, and HQL-79 displayed a mild inhibitory effect on tumor growth, but their combination was synergic (Fig. 7G and H).

We then confirmed our main findings in human systems. First, we proved that *HPGDS* was upregulated in human monocyte-derived macrophages (hMDM) stimulated by protumoral cytokines such as IL-4 and IL-10 and downregulated upon TNFα supplementation (Fig. 7I). Silencing of *HPGDS* (Supplementary Fig. S11H) in IL-4–stimulated hMDMs elicited *CXCL10* expression and downregulated *MRC1/CD206* (Supplementary Fig. S11I). Both pharmacologic and genetic inhibition of HPGDS in hMDMs unleashed CD8$^+$ T-cell migration (Fig. 7J; Supplementary Fig. S11J).

Last, the therapeutic effect of pharmacologic HPGDS inhibition was tested in melanoma patient-derived organotypic tumor spheroids (PDOTS; ref. 42). Though we tested a sample deriving from one patient only, treatment with 1 μmol/L HQL-79 for 72 hours decreased the viability of the tumoroids (Fig. 7K) and led to an accumulation of total and TNFα-producing CD8$^+$ T cells (Fig. 7L–N). HQL-79 did not affect the abundance of total TAMs (Supplementary Fig. S11K) but induced the upregulation of MHC-II (Fig. 7O). Taken together, these findings suggest that HPGDS could be a potential therapeutic target to modulate the immune response in patients with cancer.

DISCUSSION

Although our knowledge on TAM biology and heterogeneity has increased considerably (24, 34, 43–48), our data in patients and mice with melanoma show that HPGDS identifies a specific subset of macrophages. HPGDS^{high} TAMs were enriched for *VSIG4*, *C1QB*, *MS4A4A*, and *SPP1*, whereas HPGDS^{low} TAMs were enriched in *CXCL9* (as well as *CXCL10* and *CXCL11*), all genes recently shown to be associated with macrophage polarity in tumor tissues (24). HPGDS-expressing TAMs fuel the TME with PGD_2 that sustains protumoral macrophage functions and inhibits the recruitment and activation of cytotoxic T cells to the tumor core. We argue that genetic deletion of HPGDS in macrophages reeducates this TAM subset toward an antitumoral and antiangiogenic phenotype and boosts both an innate and adaptive antitumor immune response. The immunosuppressive cross-talk engaged by HPGDS-expressing macrophages requires both PGD_2 receptors, DP1 and DP2. Previous studies already investigated DP1 and DP2 as key regulators of the inflammatory response (36, 37, 49). However, their role in the context of tumor progression is unclear (50–52). In this study, we report that mostly DP1 in CD8$^+$ T cells and both DP1 and DP2 in macrophages are important to sustain tumor progression through their binding to PGD_2 produced by HPGDS$^+$ TAMs. Specifically, PGD_2 can act in an autocrine manner by promoting the anti-inflammatory behavior of macrophages. Besides this autocrine loop, PGD_2 also works in a paracrine manner through DP1 signaling in CD8$^+$ T cells, ultimately impeding their recruitment, activation, proliferation, and antitumor cytotoxic functions. Our data show that the antitumor effect achieved by HPGDS inhibition in macrophages relies, in great part, on CD8$^+$ T cells that, under low PGD_2 levels, accumulate to the tumor core and become more active. In contrast, metastasis inhibition and vessel normalization are supported by reeducated TAMs. These effects can be independently driven by TAM reeducation (53–55) but can also be partly linked because a normalized tumor vasculature can lower cancer cell intravasation and tumor hypoxia (31, 34, 56). In our system, PGD_2 inhibition was sufficient to reshape the TME despite the presence of other prostaglandins such as PGE_2 that did not change in response to HPGDS blockade. Several studies have shown that PGE_2 (signaling through EP2 and EP4) prevents the expansion of tumor-reactive T cells and effector differentiation from stem-like CD8$^+$ T cells by hindering IL-2 signaling, but it also blocks inflammatory monocyte-dictated T-cell activation in melanomas (9–11). This suggests that PGD_2 and PGE_2 have overlapping features possibly mediated by a common GPCR–Gαs–PKA signaling axis leading to T-cell dysfunction

Figure 6. Pharmacologic HPGDS inhibition phenocopies the effect of its genetic deletion in TAMs. **A–C,** Tumor growth (**A**), tumor weight (**B**), and tumor representative pictures (**C**) of YUMM 1.7 CD90.1$^+$ melanoma-bearing mice treated by oral gavage with HQL-79, 15 mg/kg BID or with vehicle control ($n = 6$). The treatment window is highlighted in pink (**A**). **D,** Fold change of *Cd80*, *Cxcl10*, *Arg1*, and *Cd206* expression in TAMs sorted from mice treated with HQL-79 or vehicle ($n = 4$). **E** and **F,** Quantification (**E**) and representative images (**F**) of F4/80 and CD80 or CD206 staining in melanoma tumors from vehicle or HQL-79–treated mice ($n = 5$). **G,** FACS analysis of YUMM 1.7 CD90.1$^+$ cancer cell intravasation into the bloodstream in melanoma-bearing mice treated by oral gavage with HQL-79 or with vehicle control ($n = 6$). **H,** qRT-PCR analysis of *Cd90.1* expression in lungs from YUMM 1.7 melanoma-bearing mice treated with vehicle or HQL-79 ($n = 5$–6). **I** and **J,** Tumor growth (**I**) and tumor weight (**J**) of YUMM 1.7 CD90.1$^+$ melanoma-bearing Ctrl or *Hpgds*$^{\Delta Mø\text{-}ERT2}$ mice treated with vehicle or HQL-79 ($n = 4$). The treatment window is highlighted in pink (**I**). **K–M,** Tumor growth (**K**), tumor weight (**L**), and tumor representative pictures (**M**) of *NRAS*^{Q61K}; *Ink4a*$^{-/-}$ melanoma tumor-bearing mice treated by oral gavage with vehicle or HQL-79 15 mg/kg BID ($n = 6$). The treatment window is highlighted in pink (**K**). **N** and **O,** Tumor growth (**N**) and tumor weight (**O**) of YUMM 1.7 CD90.1$^+$ melanoma-bearing mice treated by oral gavage with Cmpd1y 0.1 – 0.3 – 1 – 3 mg/kg BID or with vehicle ($n = 7$–9). Data show a pool of two independent experiments. The treatment window is highlighted in pink (**N**). **P** and **Q,** Tumor growth (**P**) and weight (**Q**) of YUMM 1.7 CD90.1$^+$ melanoma-bearing mice treated by oral gavage with TAS-205 30 mg/kg BID or vehicle ($n = 9$). The treatment window is highlighted in pink (**P**). *P* values are assessed by (**A**, **I**, **K**, **N**, and **P**) two-way repeated measures ANOVA, (**B**, **G**, **H**, **L**, and **Q**), unpaired, two-tailed Student *t* test, (**E**) multiple unpaired Student *t* test, (**J**) two-way ANOVA with Tukey multiple comparison test, and (**O**) one-way ANOVA with Tukey multiple comparison test. Graphs show the mean ± SEM. Scale bar: **F**, 20 μm. BID, twice daily.

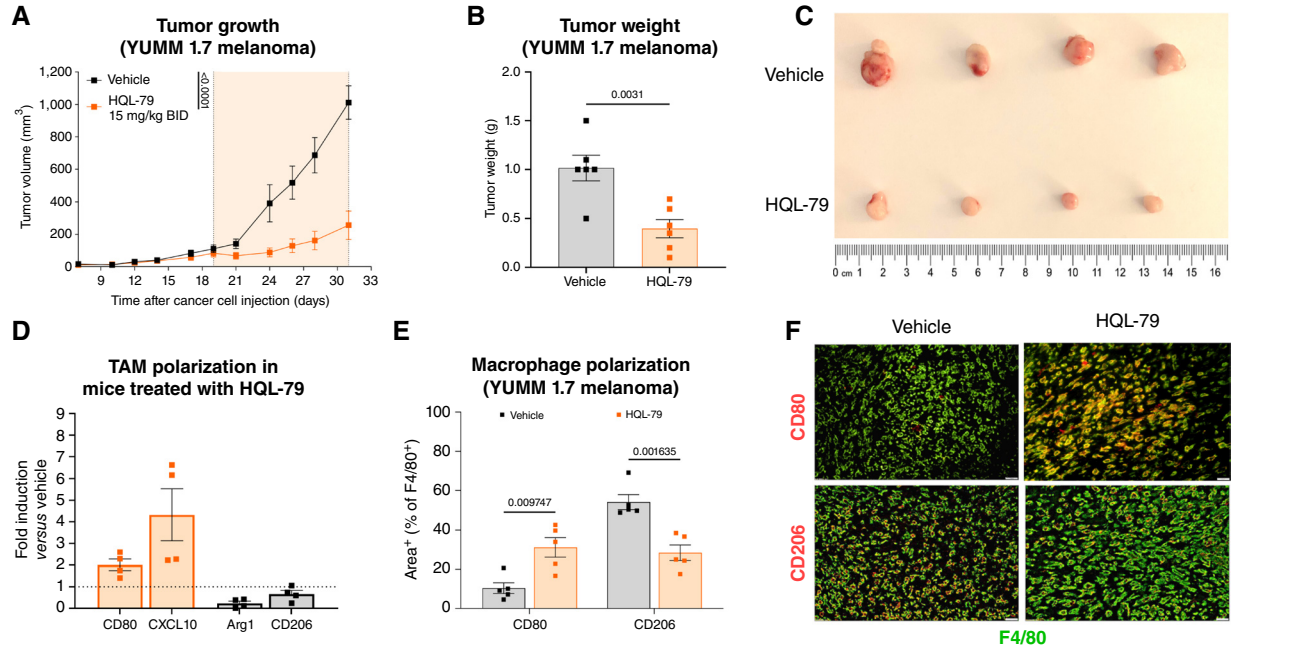

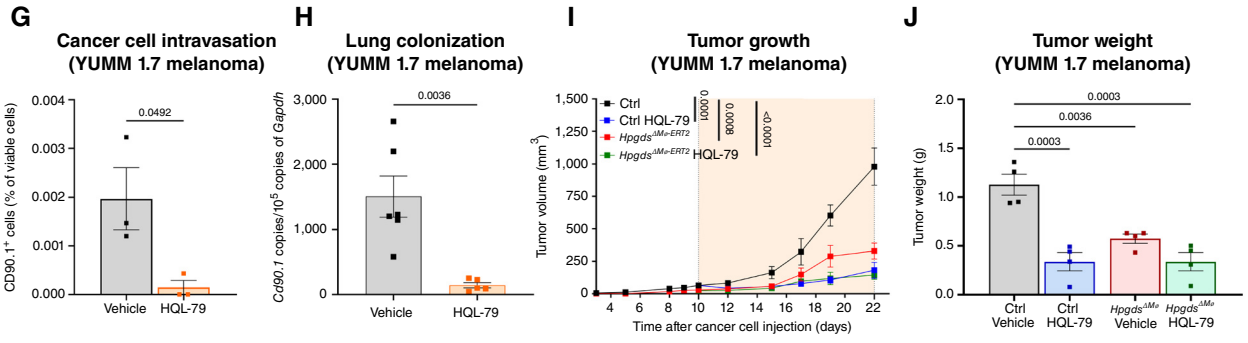

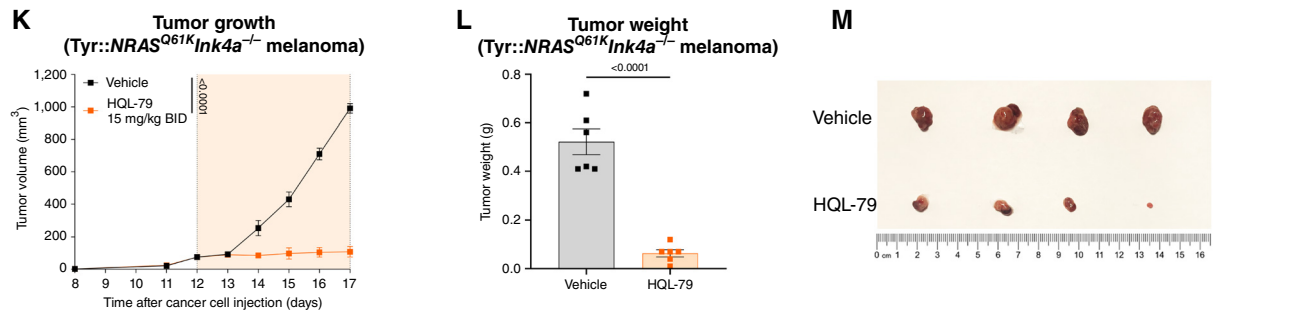

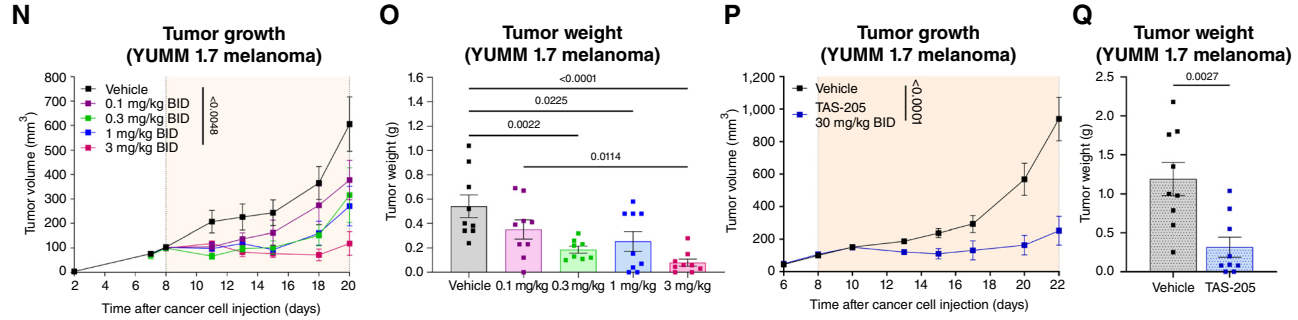

and cancer immunotherapy failure (57) but also unique biological functions as inhibition of cancer cell–killing or T-cell exclusion might be ascribed, for example, to PGD_2 only. It will be interesting to assess in the future whether EP- or DP-targeted therapy resistance is mediated by PGD_2 or PGE_2 upregulation, respectively, or whether combined EP and DP blockade shows stronger and more durable outcome than each monotherapy alone.

Our results do not contradict the observation in B16 melanomas and LLC lung carcinomas that ubiquitous *Hpgds* host deficiency enhances tumor growth through mast cell activation (20). Unlike B16 melanomas and LLC lung subcutaneous carcinomas, intradermic YUMM 1.7 melanomas have a high number of HPGDS$^+$ TAMs that represent the main cell type expressing this enzyme. The presence of a quasi-selective population of cells expressing HPGDS also reconciles our findings with previous literature showing a propermeability, proangiogenic effect of PGD_2 on ECs (58). Indeed, we argue that tumor vessel normalization is due to the phenotypic switch in HPGDS-deficient macrophages, characterized by lower levels of proangiogenic factors, e.g., FGF2 and HGF, and an increase in angiostatic CXCL9/10/11 (34, 31, 59–61, 54), rather than to the loss of PGD_2 stimulation on blood vessels, as the endothelium is prone to a self-sufficient, autocrine loop of PGD_2 produced by LPGDS (21, 62).

From a therapeutic point of view, HPGDS inhibition alone is enough to impede the progression of engrafted *Braf*- or *Nras*-mutant melanomas and to prevent tumor relapse by adding αPD1. Conversely, HPGDS-targeted therapy did not show any antitumor effect *per se* in a non–T cell–inflamed model of autochthonous melanomas harboring $Braf^{V600E/+;Pten^{-/-}}$ mutations. However, in this study, HPGDS inhibition sensitized the tumors to αPD1 treatment, likely by inducing the expansion of progenitor-exhausted (PD1$^+$) T cells (Tpex) and their recruitment to the tumor core as the result of reduced PGD_2 levels in the TME. This was mirrored *in vitro* by the inhibitory effect of PGD_2 on CD8$^+$ T-cell migration and PD1 expression. The synergism of pharmacologic HPGDS inhibition and αPD1 was also observed in pancreatic cancer, which in the clinic is almost completely unsensitive to immunotherapies.

Our data in patients with melanoma show that HPGDS-expressing TAMs remain unaltered by αPD1 treatment in NRs, suggesting that PGD_2 promotes an ICB-refractory TME. Conversely, we show, for the first time, that CD8$^+$ T-cell activation in response to αPD1 treatment shapes an immune-permissive TME by downregulating HPGDS in a specific subset of TAMs via TNFα release. TNFα has been linked to opposite phenotypes, from antitumor reprogramming of immune cells as in this or in other studies (63), to pathogenic inflammation early after cancer onset, as shown in the context of PDAC, in which TNFα together with PGE_2, promotes ILβ$^+$ tumor-initiating macrophages (64). Our experiments in mice demonstrate that preventing HPGDS downmodulation by activated T cells is sufficient to switch the TME from immunotherapy-permissive to immunotherapy-resistant. This switch involves augmented dysfunctional angiogenesis, increased cancer cell invasion, and enhanced immunosuppression. Conversely, HPGDS downregulation in macrophages triggers a feedforward loop that induces tumor vascular normalization and amplifies CD8$^+$ T-cell recruitment and activation. Together, these data support the idea of testing HPGDS inhibitors in monotherapy or in combination with αPD1 in case of primary or secondary resistance to ICB (Fig. 7P).

The clinical safety and efficacy of HPGDS-targeted therapies have been tested in numerous diseases (65–68). For example, HPGDS pharmacologic inhibition has been tested in phase III in patients with Duchenne muscular dystrophy (67) and in a phase I clinical trial to evaluate the tolerability and pharmacokinetics of an HPGDS inhibitor for the treatment of COPD, asthma, and idiopathic pulmonary fibrosis (NCT NCT02397005). Though deeper investigation is required, our initial observations suggest that HPGDS is selectively expressed by a subset of tumor macrophages but not in monocytes or tissue macrophages. This expression pattern holds promise for the development of safer therapies compared with those achieved so far with other macrophage-associated targets, such as CSF1R, whose expression in monocytes and tissue macrophages brings the risk of impairing homeostatic functions of the mononuclear phagocyte system (69, 70). Similarly, genetic targeting of DP1 and/or DP2 in TAMs and CD8$^+$ T cells supports the potential repurposing of receptor

Figure 7. HPGDS inhibition overcomes immunotherapy resistance and is effective in human settings. **A–C,** Tumor growth (**A**), tumor weight (**B**), and representative images (**C**) of $Braf^{V600E}Pten^{-/-}$ genetically engineered mice (GEM) treated with vehicle, HQL-79 15 mg/kg twice daily, αPD1, or the combination of HQL-79 and αPD1 ($n = 6$). The treatment window is highlighted in pink (**A**). **D,** Percentage of CD11c$^+$ macrophages in $Braf^{V600E}Pten^{-/-}$ GEM treated with vehicle, HQL-79, αPD1, or the combination of HQL-79 and αPD1 ($n = 6$). **E,** Flow cytometric quantification of PD1 expressing CD8$^+$ T cells in $Braf^{V600E}Pten^{-/-}$ GEM treated with vehicle, HQL-79, αPD1, or HQL-79 in combination and αPD1 ($n = 6$). **F,** Histologic quantification of CD8$^+$ T cells at the tumor margin vs. core in $Braf^{V600E}Pten^{-/-}$ GEM treated with vehicle/IgG, HQL-79, αPD1, or HQL-79 in combination with αPD1 ($n = 6$). **G** and **H,** Tumor weight (**G**) and representative pictures (**H**) of KPC FC1245 PDAC-bearing mice treated with vehicle/IgG, HQL-79, αPD1, or HQL-79 in combination with αPD1 ($n = 11$–16). **I,** qRT-PCR analysis of the expression of *HPGDS* in hMDMs Ctrl or stimulated with protumoral cytokines (i.e., IL-4 and IL-10) or first with IL-4 and then with TNFα ($n = 3$). **J,** Two hours migration of CD8$^+$ T cells through 5-μm-pore polycarbonate membranes of CD8$^+$ T cells in the presence of IL-4–polarized or Ctrl hMDMs treated with 1 μmol/L HQL-79 or with vehicle control (negative control: bottom chamber medium without macrophages; $n = 3$–6). **K** and **L,** Calcein area (**K**) and CD8$^+$ T-cell increase (**L**) of PDOTS treated with 1 μmol/L HQL-79 or with vehicle control for 72 hours. **M–O,** Flow cytometric quantification of total CD8$^+$ T cells (CD8$^+$ T cells out of CD45$^+$ cells; **M**), TNFα produced by CD8$^+$ T cells (MFI TNFα on CD8$^+$ T cells; **N**), and HLA-DR (HLA-DR^{high} out of CD68$^+$ cells; **O**) in PDOTS treated with 1 μmol/L HQL-79 or with vehicle control for 96 hours. **P,** Schematic representation of HPGDS contribution to the TME and immunotherapy response in melanoma. HPGDS-mediated PGD_2 production by TAMs results in autocrine activation of DP1 and DP2, which sustains their protumoral features, whereas PGD_2 binding to CD8$^+$ T cells blocks their recruitment and activation (**1**). TNFα released by activated T cells suppresses HPDGS transcription, as observed in ICB Rs. In turn, HPGDS downregulation and a consequent reduction in PGD_2 production favor an immune-permissive and antitumoral environment (**2**). In NRs, HPGDS-expressing TAMs inhibit T-cell activation but also promote vessel abnormalization and metastasis (**3**). Blocking HPGDS induces vascular normalization and immune surveillance, overcoming ICB resistance (**4**). *P* values are assessed by **A**, two-way repeated measures ANOVA, (**B**, **D**, **E**, and **G**) one-way ANOVA with Tukey multiple comparison test, (**F**) multiple paired Student *t* test, (**I**) one-way ANOVA with Tukey multiple comparison test, and (**J**) two-way ANOVA with Tukey multiple comparison test. Graphs show the mean ± SEM. **P,** Created with BioRender.com. Trotta, R. (2025) (https://BioRender.com/y35l375.)

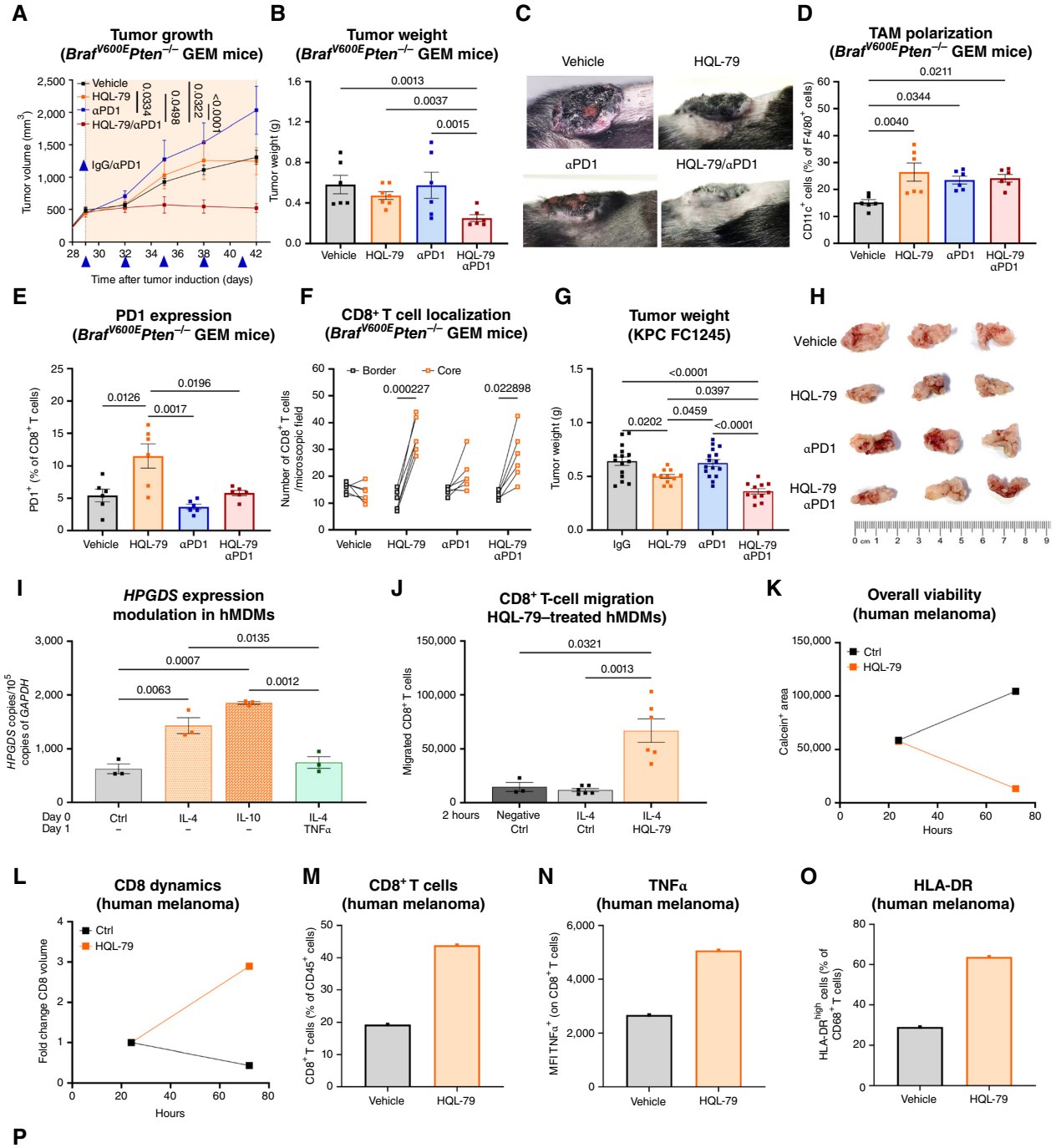

antagonists in cancer therapy. Indeed, DP1 and DP2 inhibitors (or dual DP1/DP2 blockers) have already been tested in preclinical models of intracerebral hemorrhage, chronic autoimmune disease, asthma, allergic diseases, or COVID–19 (71–74) and in patients with asthma and allergic rhinitis (75, 76) but never in the cancer context.

In conclusion, we show that HPGDS downregulation in TAMs by activated T cells controls the innate immune system and shapes the entire TME by reducing PGD_2 production. Consistently, we provide evidence that targeting the HPGDS–PGD_2–DP1/DP2 axis in melanoma sculpts TAMs away from their immunosuppressive and protumoral behavior, promoting an immune-permissive and antitumoral TME.

METHODS

Animal Strains

All experimental animal procedures were approved by the Institutional Animal Care and Research Advisory Committee of KU Leuven (P226/2017 and P012/2022). Mice were maintained under pathogen-free and temperature- and humidity-controlled conditions with a 12-hour light/12-hour dark cycle and received normal chow (sniff, R/M-H). Animals were removed from the study and killed if any signs of pain and distress were detected or if the engrafted tumor volume reached 1,000 mm^3. The maximal tumor size was not exceeded in all reported studies. OT-I mice were purchased from Taconic. Macrophage-specific *Hpgds* KO mice were generated by intercrossing the tamoxifen-inducible *Csf1r:Cre-ERT* (a kind gift of J.W. Pollard from the University of Edinburgh, Scotland) with LoxP-STOP-LoxP Cas9 mice [B6J.129(B6N)- Gt(ROSA) 26Sortm1(CAG-cas9*,-EGFP)Fezh/J], purchased from The Jackson Laboratory. $Braf^{V600E}$ $Pten^{-/-}$ mice (a kind gift of C. Marine from VIB-CCB KU Leuven, Belgium) were generated by intercrossing $Braf^{CA}$, *Tyr::Cre-ER*^{T2} mice with $Pten^{lox4-5}$ mice. The *Cre*-mediated conversion of $Braf^{CA}$ to $Braf^{VE}$ and the deletion of exons 4 and 5 was obtained by topical administration of 2 mg/mL (5 mmol/L) of 4-HT on the back skin of adult mice. The mouse line *C57BL/6N-Hpgds/Tcp* was made as part of the KOMP2-DTCC project from KOMP ES cells (77) at The Centre for Phenogenomics. It was obtained from the Canadian Mouse Mutant Repository. The NEO (neomycin) cassette was deleted *in vivo* by using FLP (flippase)-mediated recombination. The final transgenic line carries two LoxP-sites in each *Hpgds* allele. Finally, we generated Fcγr1:Cre (B6-*Fcgr1*^{tm3Ciphe}) × $Hpgds^{lox/lox}$ mice in a C57BL/6N background by intercrossing $Hpgds^{lox/lox}$ mice with the macrophage-specific Fcγr1:Cre (otherwise named CD64:Cre) deleter mouse line. CD64:Cre mice were a gift from Bernard Malissen (French National Centre for Scientific Research, CNRS). The mutant mouse line C57BL/6NTac-Fcγr1$^{tm(EGFP/Cre/ERT2)Wtsi}$/WtsiH mice (otherwise named CD64:Cre^{ERT2}) were originated by the Wellcome Trust Sanger Institute Mouse Genetics Project (Sanger MGP) and the European Mouse Mutant Archive (www.infrafrontier.eu; Repository number EM: 11125) partner at the Mary Lyon Centre at MRC Harwell from which the mouse line was received. Thus, we intercrossed CD64:Cre^{ERT2} with $Hpgds^{lox/lox}$ mice to generate the conditional $Hpgds^{\Delta M\phi\text{-}ERT2}$ mouse.

Macrophage-specific *Ptgdr1* and *Ptgdr2* KO were generated by intercrossing either $Hpgds^{lox/lox}$–CD64:Cre mice or $Hpgds^{wt/wt}$–CD64:Cre mice with LoxP-STOP-LoxP Cas9 mice [B6J.129(B6N)-Gt(ROSA) 26Sortm1(CAG-cas9*,-EGFP)Fezh/J] mice. CD8a-specific *Ptgdr1* and *Ptgdr2* KO mice were generated by intercrossing CD8a mice with LoxP-STOP-LoxP Cas9 mice [B6J.129(B6N)-Gt(ROSA) 26Sortm1(CAG-cas9*,-EGFP)Fezh/J] mice, generating CD8:specific *Ptgdr1* or *Ptgdr2* KO mice. CD8a-Cre mice were purchased from The Jackson Laboratory. All mice used for tumor experiments were females between 7 and 10 weeks old. An experiment (Fig. 2F–M) was only performed in males between 8 and 10 weeks old. WT C57BL/6N mice were obtained from the KU Leuven breeding facility.

Cell Lines

The melanoma YUMM 1.7 cell line was a kind gift from Prof. R. Marais (Manchester, United Kingdom) and cultured in DMEM/F-12 medium (Gibco, 11039021) supplemented with 10% FBS (Biowest, S00F910002), 1% (v/v) penicillin/streptomycin (Gibco, 15140-122) 2 mmol/L L-Glut (Gibco, 25030-024), and 0.1 mmol/L nonessential amino acid (NEAA; (Gibco, 11140-035). For the overexpression of OVA, the pCDH_CMV7-OVA-EFI-G418 plasmid was used. YUMM 1.7 cells were then transduced with concentrated lentiviral vectors and further selected with G418 antibiotics (1 mg/mL, Invivogen, ant-gn) to generate a homogenous population of OVA-expressing YUMM 1.7 cancer cells. The melanoma YUMMER 1.7 cell line was a kind gift from Prof. M. Bosenberg (New Haven, Connecticut) and cultured in DMEM/F-12 medium (Gibco, 11039021) supplemented with 10% FBS (Biowest, S00F910002), 1% (v/v) penicillin/streptomycin (Gibco, 15140-122), 2 mmol/L L-Glut (Gibco, 25030-024), and 0.1 mmol/L NEAA (Gibco, 11140-035). The *NRAS*-driven melanoma cell line (kindly provided by Prof. C. Marine, VIB-CCB KU Leuven) was generated by isolation of *Tyr::Cre-ER(T2); Tyr::Ink4a*$^{-/-}$*; R62R Confetti* tumors and cultured in DMEM/F-12 medium (Gibco, 11039021) supplemented with 10% FBS (Biowest, S00F910002), 1% (v/v) penicillin/streptomycin (Gibco, 15,140-122), and 2 mmol/L L-Glut (Gibco, 25030-024). The cells were incubated at 37°C in a 5% CO_2 humidified atmosphere and subcultured approximately every 3 days to maintain a log growth phase. The KPC pancreatic pancreatic cell line (FC 1245) was a kind gift from Prof. D. Tuveson and was derived from a spontaneous KPC ($Kras^{LSL.G12D/+}$; $p53^{R172H/+}$; Pdx: $Cre^{Tg/+}$) pancreatic cancer mouse model. KPC cells were cultured in DMEM medium (Gibco, 41965-039) supplemented with 10% FBS (Biowest, S00F910002), 1% (v/v) penicillin/streptomycin (Gibco, 15140-122), and 1 mmol/L sodium pyruvate (Gibco, 11360-070). Cell lines were carried out for no more than 10 cell passages in this work and regularly tested for *Mycoplasma*. Negative *Mycoplasma* contamination was verified using LookOut Mycoplasma PCR Kit (Sigma-Aldrich, MP0035) and Mycoplasma Detection Kit plus Assay Control (Lonza, LT07-705). All the cancer cell lines used were authenticated by Idexx Bioresearch.

Murine BMDMs

Murine BMDMs were derived from BM precursors as described before (44). Briefly, BM cells were cultured in a 10 cm Petri dish (non–tissue culture–treated, bacterial grade; Fisher Scientific, 12664785) in a volume of 6 mL of DMEM (Gibco, 41965-039) supplemented with 20% FBS (Biowest, S00F910002), 30% L929 CM as a source of M-CSF, 1% (v/v) penicillin/streptomycin (Gibco, 15140-122), 2 mmol/L L-Glut (Gibco, 25030-024), and 2.5% Hepes (Gibco, 15630-049). After 4 days of differentiation, the medium was removed and cells were cultured for an additional 2 days in DMEM (Gibco) supplemented with 10% FBS, 1% (v/v) penicillin/streptomycin (Gibco), and 2 mmol/L L-Glut (Gibco). At day 6, macrophages were detached with ice-cold PBS.

hMDMs

Buffy coat samples from healthy donors were obtained from the Red Cross-Flanders (institutional approval RKOV_19015), and written informed consent was obtained from all the donors. Peripheral blood mononuclear cells were isolated by Ficoll density centrifugation (Axis-Shield, 1114545) and washed in PBS containing 1 mmol/L EDTA (Sigma-Aldrich, 102461169). The ring at the interface was collected, washed with PBS (Thermo Fisher Scientific, 14190144), and

counted. Monocytes were isolated by using magnetic CD14-conjugated MicroBeads (Miltenyi Biotec, 130-050-201) and differentiated into hMDMs (44). Thus, monocytes were cultured in 6-well plates (1×10^6 cells/well in 2 mL media) in RPMI (Gibco, 21875-034) supplemented with 10% FBS (Biowest, S00F910002), 2 mmol/L L-Glut (Gibco, 25030-024), 1% penicillin/streptomycin (Gibco, 15140-122), and 25 ng/mL recombinant human M-CSF (Peprotech, 300-25) for 5 days. On the third day of differentiation, cytokines were refreshed. At day 6, macrophages were harvested in ice-cold PBS.

Mouse T-cell Isolation and Activation

Murine naïve $CD8^+$ and $CD4^+$ T cells were isolated from the spleen by processing the cells through a 40-μm cell strainer in sterile PBS (Thermo Fisher Scientific, 14190144), and cells were centrifuged for 10 minutes at 300 × *g*. Red blood cell lysis was performed by using Hybri-Max (Sigma-Aldrich, R7757). Naïve $CD8^+$ and $CD4^+$ T cells were isolated using the mouse $CD8^+$ T-cell Isolation Kit (BioLegend, 480035) or the mouse $CD4^+$ T-cell Isolation Kit (BioLegend, 480033) according to the manufacturer's instructions. For naïve T-cell activation, cells were cultured for 24 hours in T-cell medium: RPMI supplemented with 10% FBS (Biowest, S00F910002), 1% penicillin/streptomycin (Gibco, 15140-122), 1% minimum essential medium (MEM) NEAAs (Gibco, 11140-035), 25 μmol/L β-mercaptoethanol (Gibco, 31350-010), and 1 mmol/L sodium pyruvate (Gibco, 11360-070) at 37°C in a humidified atmosphere containing 5% CO_2. When indicated, T cells were activated with CD3/CD28 Dynabeads (Thermo Fisher Scientific, 11453D) at a 1:1 bead-to-cell ratio. 1 day after the activation, the beads were magnetically removed, and activated $CD8^+$ T cells were further expanded in the T-cell medium supplemented with 30 U ml^{-1} mIL-2 (Peprotech, 212-12).

Human $CD8^+$ T-cell Isolation and Activation

Buffy coat samples from healthy donors were obtained from the Red Cross-Flanders (institutional approval RKOV_19015) and written informed consent was obtained from all the donors. Peripheral blood mononuclear cells were isolated by Ficoll density centrifugation (Axis-Shield, 1114545) and washed in PBS containing 1 mmol/L EDTA (Sigma-Aldrich, 102461169). The ring at the interface was collected, washed with PBS (Thermo Fisher Scientific, 14190144), and centrifuged for 10 minutes at 300 × *g*. Naïve $CD8^+$ T cells were isolated by using the human $CD8^+$ T-cell Isolation Kit (BioLegend, 480129) according to the manufacturer's instructions. T cells were then activated in T-cell medium: RPMI supplemented with 10% FBS (Biowest, S00F910002), 1% penicillin/streptomycin (Gibco, 15140-122), 1% MEM NEAAs (Gibco, 11140-035), 25 μmol/L β-mercaptoethanol (Gibco, 31350-010), and 1 mmol/L sodium pyruvate (Gibco, 11360-070) by adding human anti-CD3/CD28-coated Dynabeads (Thermo Fisher Scientific, 11132D) at a 1:1 bead-to-cell ratio. The day after activation, the beads were magnetically removed and $CD8^+$ T cells were expanded in the T-cell medium supplemented with recombinant human IL-2 (PeproTech, 200-02).

HUVECs

HUVECs were freshly isolated from umbilical cords obtained from multiple donors (with approval from the Ethics Committee Research UZ/KU Leuven, and written informed consent obtained from all subjects was obtained) as previously described (44, 78) and regularly tested for *Mycoplasma*. They were maintained in M199 medium (Gibco, 12340-030) supplemented with 20% FBS (Biowest, S00F910002), 2 mmol/L L-Glut (Gibco, 25030-024), 1% penicillin/streptomycin (Gibco, 15140-122), 0.15% heparin, and 20 μg/mL endothelial cell growth supplement (ECGS, PromoCell, C-30160). 0.1% type B gelatin (Sigma-Aldrich, G1393) was used to stimulate the adhesion of HUVECs to the flask bottom.

Patients with Human Melanoma and PDAC

Paraffin-embedded tumor samples from patients with melanoma and PDAC were analyzed histologically for CD8 (Agilent, GA623, RRID: AB_3073940; only in R/OT and NR/OT patients with melanoma) and for HPGDS (R&D Systems, MAB6487, RRID: AB_10972458) in $CD163^+$ (Leica Biosystems, NCL-L-CD163, RRID: AB_2756375) macrophages. The clinical protocol was approved by the Ethical Committee of the University Hospitals Gasthuisberg KU Leuven (S62275 and ML3452 for melanoma and PDAC, respectively), and written informed consent from all subjects before study participation was obtained. Detailed tumor characteristics for patients with melanoma are listed in Supplementary Table S1.

Tumor Models

1×10^6 YUMM 1.7 or 1×10^6 *NRAS*-driven melanoma cell lines, genetically engineered by lentiviral transduction to express CD90.1, were injected intradermally in the right flank of the mouse in a final suspension of 50 μL PBS. In the experiment described in Fig. 2G (in which the comparison between Rs and NRs with melanoma was performed) 1.2×10^6 YUMM 1.7 WT cells were intradermally injected in the right flank of the mouse in a final suspension of 50 μL PBS. The 1.2×10^6 YUMMER 1.7 melanoma cell line was injected intradermally in the right flank of the mouse in a final suspension of 50 μL PBS. For the genetically engineered mouse melanoma model ($Braf^{V600E}$ $Pten^{-/-}$), topical administration with 2 mg/mL (5mmol/L) of 4-HT (Sigma-Aldrich, H7904) on the back skin of adult mice was performed. Tumor volumes were measured three times a week with a caliper and calculated using the following formula: $V = \pi \times (d2 \times D) / 6$, in which *d* is the minor tumor axis and D is the major tumor axis. 0.4×10^6 KPC FC1245 cell lines were injected orthotopically into the head of the pancreas in 20 μL of PBS. Six days after tumor injection, mice were randomized based on body weight.

In Vivo Treatments

For the TNFα inhibition *in vivo*, mice were randomized when the average tumor volume was 100 mm^3 and treated intraperitoneally three times per week until the end of the experiment with 10 mg/kg of Enbrel (Etanercept; Pfizer) or human IgG (Sigma-Aldrich, I4506, RRID: AB_1163606). For the treatment with αPD1 (BioLegend, 114122, RRID: AB_2800578), mice were randomized when the average of the tumor volumes was 150 mm^3 and treated intraperitoneally two times per week with 10 mg/kg αPD1 or control IgG from rat serum (Sigma-Aldrich, I4131, RRID: AB_1163627). For CD4 depletion, mice were treated 3 days before tumor injection (500 μg/mouse) and then two times per week (250 μg/mouse) until the end of the experiment with αCD4 (Bio X Cell, BE0003-1, RRID: AB_1107636). The efficiency of CD4 depletion was assessed by FACS in the blood. For CD8 depletion, mice were treated intraperitoneally with 5 mg/kg αCD8 (Bio X Cell, BE0117, RRID: AB_10950145) or control IgG from rat serum. Treatment with αCD8 was performed 3 days before tumor injection and then one time per week until the end of the experiment. The efficiency of CD8 depletion was assessed by FACS in the tumor. For the pharmacologic inhibition of HPGDS, mice were treated by oral gavage with HQL-79 (Cayman Chemical Company, 10134, RRID: AB_3662692; 15 mg/kg twice daily), 1,8-naphthyridine 1y (in short, Cmpd1y; GSK; 0.1–0.3–1–3 mg/kg twice daily), TAS-205 MedChemExpress, HY-109134A, RRID: AB_3662693; 30 mg/kg twice daily), or control vehicle (methylcellulose). For the engrafted melanoma mouse models, mice were randomized when the average tumor reached 100 mm^3 and treated two times per day with the indicated compound. For the genetically engineered mouse melanoma model, treatment with HQL-79 15 mg/kg twice daily, αPD1 10 mg/kg, the combination of both, or vehicle and IgG started when the average tumor volume was 500 mm^3).

The acute deletion of *Hpgds* in macrophages in *Hpgds*$^{\Delta M\phi\text{-}ERT2}$ mice was obtained by intraperitoneal injection of tamoxifen (Sigma-Aldrich, T5648; 1 mg/mouse/day) for five consecutive days (from day -7 to day -2) prior to intradermal injection of YUMM 1.7 CD90.1$^+$ melanoma cancer cells. Mice were then treated with tamoxifen until the end of the experiment (5 days/week) and with HQL-79 15 mg/kg twice daily or with control vehicle (methylcellulose).

For the KPC model, 6 days after tumor injection, mice were treated intraperitoneally with 10 mg/kg αPD1 and control IgG from rat serum. For the pharmacologic inhibition of HPGDS, mice were treated for 9 days by oral gavage with HQL-79 15 mg/kg twice daily or control vehicle (methylcellulose).

BM Transplantation and Generation of Hpgds KO Chimeras

For the generation of *Hpgds* KO→ WT mice, the stop-floxed Cas9 knock-in line (79) was intercrossed with Csf1r:Cre-ERT mice (80) allowing the inducible expression of the Cas9 nuclease in monocytes and macrophages only (donor mice). Thus, 7- to 8-week-old recipient mice were lethally irradiated with a dose of 9.2 Gy using the Small Animal Radiation Research Platform (SARRP, XSTRAHL). The same day, after cervical dislocation, femur, tibia, and humerus were collected from donor mice. The BM was obtained by flushing the bones with a syringe filled with DMEM supplemented with 10% FBS. The cells were subsequently filtered twice by using a 40-μmol/L-pore-sized mesh and centrifuged for 10 minutes at 300 × *g*. BM were counted and resuspended 1 × 10^8 cells/mL. EasySep Mouse Hematopoietic Progenitor Cell Isolation Kit (19856, STEMCELL Technologies) was used to isolate lineage-negative hematopoietic stem cells according to the manufacturer's instructions. Cells were stimulated for 4 hours in StemSpan serum-free medium (STEMCELL Technologies, 09650) with 20 ng/mL IL-3 (Peprotech, 213-13), 100 ng/mL SCF (Peprotech, 250-03), 100 ng/mL TPO (Peprotech, 315-14), and 100 ng/mL FLT-3L (Peprotech, 250-31) and then transduced with a specific guide RNA (gRNA; *5′*-AGATATTTGACCAAAAACAC-*3′*), enabling the investigation of the *Hpgds* in a monocyte/macrophage-specific and inducible fashion. For the nontargeting condition (WT → WT) the following gRNA was used *5′*-GAACAGTCGCGTTTGCGACT-*3′*. A multiplicity of infection reaching approximately 30% of transduction was used. After a double spin infection, cells were counted, and 1 × 10^6 cells were injected intravenously via the tail vein in the irradiated recipient mice. Specifically, for *Hpgds* KO → WT mice, the deletion was achieved by intraperitoneal injections of tamoxifen (Sigma-Aldrich, T5648; 1 mg/mouse/day) for five consecutive days. Red and white blood cell count was determined by flow cytometry on peripheral blood collected in heparin with capillary pipettes by retro-orbital bleeding. Tumor experiments were initiated 5 to 6 weeks after immune reconstitution. The efficiency of HPGDS deletion was confirmed *in vivo* by immunofluorescence on primary tumor and *in vitro* by WB on BMDMs. For both readouts the following antibody was used: rat anti-HPGDS (Cayman Chemical Company, 10004348, RRID: AB_10079369). For the *in vitro* validation, BMDMs (derived from *Csf1r:Cre-ERT* x LoxP-STOP-LoxP Cas9 mice) were isolated as described before (44). 1 × 10^6 cells were seeded in a 6-well plate and, after 3 days, transduced with a vector containing the gRNA targeting the *Hpgds* locus or a nontargeting control gRNA. The day after, the medium was refreshed, and cells were treated with 2 μg/mL 4-HT (Sigma-Aldrich, H7904). At day 6, cells were treated for the second time with 2 μg/mL 4-HT. Cells were collected and WB was performed at day 8.

Generation of Ptgdr1/Ptgdr2 KO Mice

For the depletion of *Ptgdr1* and *Ptgdr2* in macrophages, the stop-floxed Cas9 knock-in line (79) was intercrossed with CD64-Cre, generating a mouse cell line in which the Cas9 nuclease was constitutively expressed in macrophages. Whereas for the KO of *Ptgdr1* and *Ptgdr2* in CD8$^+$ T cells, Cas9 knock-in mice were intercrossed with *CD8a*-Cre mice, allowing the constitutive depletion of the two target genes only in CD8$^+$ T cells. The gRNAs used to target *Ptgdr1 or Ptgdr2* are listed as follows in *5′-3′* orientation: *Ptgdr1* CACGAGCACAT AAAAGACCG, *Ptgdr2* TGTTCAGAGACACCATCCCG, no-targeting gRNA, and GAACAGTCGCGTTTGCGACT (these gRNAs were used for the generation of both single- and dual-KO mice). The experimental setting described above was applied for the generation of *Ptgdr1* and *Ptgdr2* KO mice. Gene deletion was confirmed at the mRNA level by using the primers described in the primer section.

HPGDS Overexpression

For the overexpression of *Hpgds* in TAMs, a plasmid containing the macrophage-specific *CD68* promoter was used (plasmid #34837, Addgene). The pRRLSIN.cPPT.hCD68L-GFP.WPRE lentiviral vector was generated by replacing the PGK sequence in the pRRLSIN.cPPT.PGK-GFP.WPRE vector (plasmid #12252, Addgene). The ORF of *Hpgds* was amplified from a cDNA derived from IL-4–polarized macrophages, thus generating pRRLSIN.cPPT.hCD68L-HPGDS.WPRE vector. Hematopoietic stem cells were transduced as described above.

Tissue Dissociation

YUMM 1.7 melanomas were harvested and minced in αMEM medium (Lonza, BE12-169F) supplemented with 5% FBS (Biowest, S00F910002), 1% penicillin/streptomycin (Gibco, 15140-122), 50 μmol/L β-mercaptoethanol (Gibco, 31350-010), 5 U/mL DNase I (Sigma-Aldrich, R5503), 0.85 mg/mL collagenase V (collagenase from clostridium histolyticum, Sigma-Aldrich, C9263), 1.25 mg/mL collagenase D (Sigma-Aldrich, 11088866001), and 1 mg/mL Dispase II (Gibco, 17105041) and digested for 30 minutes at 37°C. Digested tissues were filtered using first a 70-μm and then a 40-μm mesh strainer.

Spontaneous tumors from *Braf*^{V600E} *Pten*$^{-/-}$ mice were harvested and minced in RPMI (Gibco, 21875-034) supplemented with 5% FBS (Biowest, S00F910002), 300 μg/mL Liberase (Sigma-Aldrich, 5401160001), and 1 μg/mL DNase I (Sigma-Aldrich, R5503) and digested for 45 minutes at 37°C. The single-cell suspension was then passed through a 40-μm strainer and red blood cells were lysed by using a Hybri-Max solution (Sigma-Aldrich, R7757).

Tumor Interstitial Fluid

YUMM 1.7 tumor explanted from *Hpgds*$^{\Delta M\phi}$ and Ctrl mice were cut into small pieces and then inserted in collection tubes (2 mL Eppendorf with five holes at the bottom in a 15-mL falcon tube). Forty μL of 9 g/L NaCl, pH 7.4, was added on top of the tumor samples before a 10 minutes centrifugation at 110 × *g* at 4°C. The interstitial fluid was collected in new vials and further used to assess lipid metabolites and mediators by LC/MS-MS on a Nexera X2 UHPLC system (Shimadzu).

TCM

YUMM 1.7 tumor explanted from WT mice was minced in 12 mL DMEM/F-12 medium (Gibco, 11039021), supplemented with 1% penicillin/streptomycin (Gibco, 15140-122), and incubated at 37°C for 72 hours. After that, the medium was filtered, and the cell-free supernatant was supplemented with 20 mmol/L HEPES (15630-049, Gibco) and 2 mmol/L of L-Glut (Gibco, 25030-24) and stored at −20°C.

TAM-like Macrophages

To differentiate BMDMs toward TAM-like cells, 4 × 10^6 BMDMs were seeded in 6-well plates in DMEM (Gibco, 41,965-039) supplemented with 10% FBS (Biowest, S00F910002), 1% penicillin/streptomycin (Gibco, 15140-122), and 20% TCM for 12 hours at 37°C in a 5% CO_2 humidified atmosphere, as previously described.

HPGDS Regulation in BMDMs

BMDMs were isolated as described before. At day 6, BMDMs were stimulated for 24 hours with 20 ng/mL IFNγ (Peprotech, 315-05) and 100 ng/mL LPS (Sigma-Aldrich, L2630), 10 ng/mL IL-4 (eBioscience, 14-8041-62), 10 ng/mL IL-6 (Peprotech, 216-16), or 5 ng/mL IL-10 (Peprotech, 210-10). To investigate the regulation of HPGDS, 24 hours after IL-4 polarization, macrophages were treated for an additional 24 hours with 20 ng/mL IFNγ, 10 ng/mL TNFα (Peprotech, 315-01A), or 100 ng/mL LPS, alone or in combination. Unstimulated BMDMs were used as controls. *Hpgds* expression level was checked by qPCR.

PGD_2 Release by Macrophages

BMDMs were isolated as described before. At day 1×10^6 macrophages were seeded in a 24-well plate and stimulated or not for 24 hours with 10 ng/mL IL-4 (eBioscience, 14-8041-62). IL-4–polarized macrophages were then treated for an additional 24 hours with 10 ng/mL TNFα (Peprotech, 315-01A). After that, medium was replaced with 200 μL of complete DMEM and conditioned for an additional 48 hours. The day of the collection, secreted PGD_2 was stabilized by adding methoxime and measured with PGD_2-MOX ELISA Kit (Cayman Chemical, 512011) in accordance with the manufacturer's protocol.

HPGDS Regulation in hMDMs

hMDMs were obtained from healthy donor buffy coats and isolated with CD14-conjugated MicroBeads (Miltenyi Biotec, 130-050-201) as described before. At day 6, hMDMs were stimulated for 24 hours with 20 ng/mL IL-4 (Peprotech, 200-04) or 40 ng/mL IL-10 (Peprotech, 200-10). Unstimulated hMDMs were used as controls. After 24 hours of stimulation, IL-4–polarized macrophages were treated for an additional day with 10 ng/mL TNFα (Peprotech, 300-01A). *HPGDS* expression level was checked by qPCR.

hMDMs Transfection

HPGDS silencing was achieved by transfecting hMDMs with specific siRNAs. Briefly, 1×10^6 hMDMs were transfected by using Lipofectamine RNAiMAX Transfection Reagent (Thermo Fisher Scientific, 13778075). A measure of 10 pmols of each of three siRNAs and the relative control were resuspended in 100 μL of Opti-MEM (Gibco, 51985-026) supplemented with 2 μL of Lipofectamine and incubated for 20 minutes at room temperature (RT). Six hours after lipofection, the medium was replaced with RPMI (Gibco, 21875-034) supplemented with 10% FBS (Biowest, S00F9110002), 1% penicillin/streptomycin (Gibco, 15140-122), and 2 mmol/L L-Glut (Gibco, 25030-024). Upon 48 hours of incubation at 37°C in a 5% CO_2 humidified atmosphere, qPCR and flow cytometric analysis were performed. Commercially available siRNAs targeting *HPGDS* were purchased from IDT (Integrated DNA Technologies, hs.Ri.HPGDS.13.1, hs.Ri.HPGDS.13.2, and hs.Ri.HPGDS.13.3). Nontarget scramble control was purchased from Qiagen (Cat: 1027310).

PGD_2 Supplementation to IL-4 Macrophages

A measure of 1×10^6 IL-4–polarized macrophages (Ctrl or $Hpgds^{\Delta M\phi}$) were seeded in 24-well plates in DMEM supplemented with 2% FBS (Biowest, S00F9110002) and 1% penicillin/streptomycin (Gibco, 15140-122) 24 hours before the addition of 1 μmol/L of PGD_2 (Cayman Chemical, 12010). Cells were then cultured for an additional 24 hours in the presence or not of PGD_2. The effect of PGD_2 was assessed at the mRNA level.

In Vitro T-cell Coculture with Macrophages

Twenty four hours before starting the coculture, IL-4–polarized or Ctrl macrophages were collected, seeded in 24-well plates, and incubated overnight at 37°C in a 5% CO_2 humidified atmosphere. When indicated, macrophages were pretreated for 24 hours with 1 μmol/L of PGD_2 (Cayman Chemical, 12010). To obtain T-cell CM, 1×10^6 activated $CD4^+$ T cells or $CD8^+$ T cells were cultured in a 6-well plate 24 hours in T-cell medium: RPMI supplemented with 10% FBS, 1% penicillin/streptomycin, 1% MEM NEAAs (Gibco, 11140-035), 25 μmol/L β-mercaptoethanol (Gibco, 31350-010), and 1 mmol/L sodium pyruvate (Gibco, 11360-070). IL-4–polarized or Ctrl macrophages were then cultured with 250 μL T-cell CM for 24 hours at 37°C in a 5% CO_2 humidified atmosphere. In the coculture experiment, macrophages were cocultured with activated $CD4^+$ T cells or $CD8^+$ T cells in a 1:1 ration and incubated 24 hours at 37°C in a 5% CO_2 humidified atmosphere. When indicated, 25 μg/mL αTNFα, 20 μg/mL αIFNγ (Miltenyi Biotech, 130-095-729), or isotype Ctrl were added to the medium. Upon the indicated time of incubation, qPCR to assess *Hpgds* expression in macrophages was performed.

PGD_2 Supplementation to $CD8^+$ T Cells

1×10^6 activated $CD8^+$ T cells were cultured in a 6-well plate 24 hours in T-cell medium (RPMI supplemented with 10% FBS, 1% penicillin/streptomycin, 1% MEM NEAAs, 25 μmol/L β-mercaptoethanol, and 1 mmol/L sodium pyruvate) before the addition of 1 μmol/L of PGD_2 (Cayman Chemical, 12010). Cells were then cultured for an additional 4 hours in the presence or absence of PGD_2. Upon the indicated time of incubation, flow cytometry to assess cytokine production (i.e., GZMB, TNFα, and IFNγ), activation status (i.e., CD69), and PD1 expression were performed.

$CD8^+$ T-cell Proliferation

OVA-specific OT-I $CD8^+$ T cells pr-activated with 1 μg/mL "SIINFEKL" peptide (IBA Lifesciences, 6-7015-901) cultured with 10 ng/mL IL-2 (Peprotech, 212-12) were treated for 4 hours with 1 μmol/L PGD_2 (Cayman Chemical, 12010) and then labeled with 5 μmol/L CellTrace Violet (Invitrogen, C34571) for 15 minutes at 37°C. OT-I–expressing cells were then cocultured with preseeded OVA-expressing YUMM 1.7 for 24 hours in the presence of 1 μmol/L PGD_2 at a 2:1 ratio (2 $CD8^+$ T cells:1 cancer cell). Cells were then stained with viability dye. Data were collected using BD FACSDiva and analyzed by FlowJo (TreeStar).

$CD8^+$ T-cell Cytotoxicity

OVA-specific OT-I $CD8^+$ T cells preactivated with 1 μg/mL "SIINFEKL" peptide (IBA Lifesciences) cultured with 10 ng/mL IL-2 (Peprotech, 212-12) were treated for 4 hours with 1 μmol/L PGD_2 (Cayman Chemical, 12010) and then labeled then cocultured with preseeded OVA-expressing YUMM 1.7 in the presence of 1 μmol/L PGD_2 for 24 hours at a ratio 2:1 (two $CD8^+$ T cells:1 cancer cell). $CD8^+$ T-cell cytotoxicity activity was determined using Cytotoxicity Detection LDH Kit (Roche, 11644793001) according to the manufacturer's instructions.

$CD8^+$ T-cell Migration

Migration of $CD8^+$ T cells was assessed by using a 5-μm-pore polycarbonate membrane (Transwell; Costar, 3387). When indicated $CD8^+$ T cells were pretreated with 1 μmol/L PGD_2 (Cayman Chemical, 12010) for 4 hours. The bottom chamber contained T-cell medium with or without 20 ng/mL CXCL10 (Peprotech, 250-18) or 2×10^5 IL-4–polarized Ctrl or $Hpgds^{\Delta M\phi}$ BMDMs pretreated or not with 1 μmol/L PGD_2 for 24 hours. Twelve hours before starting the assay, $CD8^+$ T cells and macrophages were cultured in T-cell medium: RPMI supplemented with 2% FBS, 1% penicillin/streptomycin, 1% MEM NEAAs (Gibco, 11140-035), 25 μmol/L β-mercaptoethanol, and 1 mmol/L sodium pyruvate (Gibco, 11360-070). Subsequently, 2×10^5 $CD8^+$ T cells were seeded and incubated for 2 hours. The migrated cells were collected and counted under the microscope.

Human CD8+ T-cell Migration

Migration of CD8+ T cells was assessed by using a 5-μm-pore polycarbonate membrane (Transwell; Costar, 3387). The bottom chamber contained 2 × 10^5 hMDMs silenced or not for *HPGDS* (negative Ctrl: T-cell medium) or pretreated or not for 24 hours with 1 μmol/L HQL-79 (Cayman Chemical Company, 10134, RRID: AB_3662692; negative Ctrl: T-cell medium with HQL-79). Twelve hours before starting the assay, CD8+ T cells and macrophages were cultured in T-cell medium: RPMI supplemented with 2% FBS, 1% pen/streptomycin, 1% MEM NEAAs (Gibco, 11140-035), 25 μmol/L β-mercaptoethanol, and 1 mmol/L sodium pyruvate (Gibco, 11360-070). Subsequently, 2 × 10^5 CD8+ T cells were seeded and incubated for 2 hours. The migrated cells were collected and counted under the microscope.

YUMM 1.7 Migration Assay

In the cancer migration assays, 8 × 10^4 YUMM 1.7 melanoma cancer cells were seeded on 8-μm-pore polycarbonate membranes (Transwell; Costar, 3422). The bottom chamber contained DMEM/F-12 (Gibco, 11039021) supplemented with 2% FBS, 1% penicillin/streptomycin and 1% L-Glut containing or not 1 μmol/L PGD_2 (Cayman Chemical, 12010). DMEM/F-12 0.2% FBS was used as a negative control. For the coculture with macrophages, the bottom chamber contained 2 × 10^5 IL-4–polarized macrophages (Ctrl or $Hpgds^{\Delta M\phi}$). Twelve hours before starting the assay, YUMM 1.7 and BMDMs were cultured in DMEM/F-12 with 2% FBS, 1% penicillin/streptomycin, and 1% L-Glut. Subsequently, cells were seeded and incubated for 12 hours. The nonmigrated cells were removed from the top of each membrane using a cotton stick. The migrated cells were fixed in 4% PFA, washed in PBS, stained with crystal violet (2.5 g/L), and mounted on glass slides. Images were acquired using an Olympus BX41 microscope and CellSense imaging software.

HUVEC Migration Assay

Twenty four hours before starting the assay, HUVECs were starved in DMEM/F-12 (Gibco, 11039021) supplemented with 2% FBS, 1% penicillin/streptomycin, and 1% L-Glut. For the macrophage CM, 500.000 IL-4–polarized macrophages (Ctrl or $Hpgds^{\Delta M\phi}$) were seeded in 600 μL of DMEM (Gibco, 1103902) supplemented with 0.1% FBS, 1% penicillin/streptomycin, and 1% L-Glut in a 24-well plate and incubated for 48 hours. For the experiment shown in Supplementary Fig. S7F, 50.000 HUVECs were seeded on 8-μm-pore polycarbonate membranes (Costar, 3422) in DMEM (Gibco, 1103902) supplemented with 0.1% FBS, 1% penicillin/streptomycin, and 1% L-Glut. The bottom chamber contains CM with or without 10 ng/mL FGF2 (Peprotech, 100-18B) or 10 ng/mL HGF (Peprotech, 100-39). Chambers were incubated for 5 hours at 37°C in a CO_2 incubator. For the experiment shown in Fig. 5G and Supplementary Fig. S7G, 50.000 HUVECs were seeded on 8-μm-pore polycarbonate membranes (Costar, 3422) in CM and incubated with or without 500 nmol/L AMG 487 (MedChemExpress, HY-15319; RRID: AB_3675858). Two hours later, 10 ng/mL VEGF (Peprotech, 100-20) was added to the lower chambers. Migration was assessed after 8 hours incubation at 37°C in a CO_2 incubator. The nonmigrated cells were removed from the top of each membrane using a cotton stick. The migrated cells were fixed in 4% PFA, washed in PBS, stained with crystal violet (2.5 g/L), and mounted on glass slides. Images were acquired using an Olympus BX41 microscope and CellSense imaging software.

Sprouting Assay

Hybrid multicellular microspheres were generated by mixing or not HUVECs and IL-4–polarized macrophages, silenced or not for *Hpgds*, in a 1:1 ratio (1,400 BMDMs and 1,400 HUVECs) and incubated overnight in hanging drops in EGM-2 (Lonza, CC-3202) medium supplemented with 20% methylcellulose 4,000 cP (Sigma-Aldrich, M0512). After harvesting the spheroids, they were embedded in collagen I gel and maintained at 37°C for 18 hours to induce sprouting. To assess the effect of PGD_2 on HUVECs, 1,400 HUVECs were harvested and incubated overnight in hanging drops of 24 μL in EGM-2 medium. Then, spheroids were embedded in collagen type I gel in a 24-well plate and cultured for 18 hours with 50 ng/mL VEGF (Peprotech, 100-20), 1 μmol/L PGD_2 (Cayman Chemical, 12010), the combination of both, or in EGM-2 medium only. Cultures were then fixed with 4% PFA at RT. Images were taken with a Leica DMI6000 microscope. The CellSense imaging software was used to analyze the number of sprouts per spheroid and the total sprout length (represented by the cumulative length of primary sprouts and branches per spheroid).

Gene Expression Analysis

To assess gene expression, cells were washed in PBS, collected in RLT buffer (Qiagen, 79216), and stored at −80°C. Lung tissue was ribolysed in TRIzol (Thermo Fisher Scientific, 15596026), extracted with chloroform, and subsequently isolated. RNA from cells or from tissue was extracted using RNeasy Mini Kit (Qiagen, 74106) according to the manufacturer's instructions. Reverse transcription to cDNA was performed with the SuperScript III and SuperScript IV First Strand cDNA Synthesis System (Invitrogen, 18080051 and 18091050, respectively) according to the manufacturer's protocol. cDNA, primer/probe mix, and PowerUp SYBR Green Mix (Applied Biosystems, A25741) or TaqMan Fast Universal PCR Master Mix (Applied Biosystems, 4352042) were prepared in a volume of 20 μL or 10 μL according to manufacturer's instructions and pipetted into an optical 96-well Fast Thermal Cycling plate (Applied Biosystems, 4346906). Analysis was performed by using the QuantStudio 12K Flex Real-Time PCR System (Applied Biosystems). Gene transcription was presented as number of gene mRNA copies relative to the housekeeping gene or as fold increase/decrease versus control. All reactions were run in duplicate.

Primers/Probes

Murine primers used for RT-qPCR are listed as follows in 5′-3′ orientation: *mGapdh* [forward (Fw) GTGGAGTCATACTGGAACA TGTAG, reverse (Rev) AATGGTGAAGGTCGGTGTG)], m*Hpgds* (Fw TGGGAAGACAGCGTTGGA, Rev AGGCGAGGTGCTTG ATGTG), *Ptgdr1* (Fw TTTGGGAAGTTCGTGCAGTACT, Rev GCCATGAGGCTGGAGTAGA), *Ptgdr2* (Fw TGGCCTTCTTCA ACAGCGT, Rev ACGCAGTTGGGGAATTCG), *Lpgds* (Fw CCTC AATCTCACCTCTACCTTCC,RevTCATAGTTGGCCTCCACCAC), *Cd90.1* (Fw GGATGAGGGCGACTACTT, Rev ACTTGACCA GCTTGTCTCTATAC), *Aqp1* (Fw AGGCTTCAATTACCCACT GGA, Rev GTGAGCACCGCTGATGTGA), *Hgf* (Fw GTCCTGAA GGCTCAGACTTGGT, Rev CCAGCCGTAAATACTGCAAGTGG), *Vegfa* (Fw TGCCAAGTGGTCCCAGGCTGC, Rev CCTGCACA GCGCATCAGCGG), *Fgf2* (Fw AAGCGGCTCTACTGCAAGAACG, Rev CCTTGATAGACACAACTCCTCTC), *Mmp9* (Fw GCAAGG GGCGTGTCTGGAGATTC, RevGCCCACGTCGTCCACCTGGTT), *Cd206* (Fw GTTCACCTGGAGTGATGGTTCTC, Rev AGGAC ATGCCAGGGTCACCTTT), *Angpt1* (Fw CATTCTTCGCTGCC ATTCTG, Rev TGCAGAGCGTTGGTGTTG), *Npr1* (Fw GCTTG TGCTCTATGCAGATCG, Rev TCGACGAACTCCTGGTGATTTA), *Hapln1* (Fw TACTGCTGTGGTGGCATTGGAG, Rev GGTCAAA GGAAGCAATCACTGCG), *Pik3cg* (Fw GCTCTTCGCCATCACAC AAAC, Rev GGCATTCCTGTCATCAGCATC), *Cxcl9 (Fw GAAC CCTAGTGATAAGGAATGCA,* Rev *CTGTTTGAGGTCTTTGAGGGATT), Cxcl10* (Fw ATCATCCCTGCGAGCCTATCCT, Rev GACCTTTT TTGGCTAAACGCTTTC), *Cxcl11 (Fw CCGAGTAACGGCTGCGA*

CAAAG, Rev CCTGCATTATGAGGCGAGCTTG), Cd11c (Fw TGC CAGGATGACCTTAGTGTCG, Rev CAGAGTGACTGTGGTTCCG TAG), and *Cd80* (Fw CCTCAAGTTTCCATGTCCAAGGC, Rev GAGGAGAGTTGTAACGGCAAGG). Murine probes *Hprt* (Mm. PT.58.32092191), *Cd80* (Mm.PT.58.10255942), *Cxcl10* (Mm. PT.58.43575827), *Arg1* (Mm.PT.58.8651372), and *Cd206* (Mm. PT.47.7673017) were used. Human primers used are listed as follows in 5'-3' orientation: *GAPDH* (Fw TGGTATCGTGGAAGGAC TCATGAC, Rev ATGCCAGTGAGCTTCCCGTTCAGC), *HPGDS* (Fw CCCCATTTTGGAAGTTGATG, Rev TGAGGCGCATTATA CGTGAG), *CXCL10* (Fw GTGGCATTCAAGGAGTACCTC, Rev TGATGGCCTTCGATTCTGGATT), and *CD206* (Fw GGGTTG CTATCACTCTCTATGC, Rev TTTCTTGTCTGTTGCCGTAGTT). For CRISPR KOs, primers are listed as follows in 5′-3′ orientation: *Ptgdr1* (Fw GCCAGAGGCACTATCCTCAC, Rev CACTGTCATG AGAGCCAGCA), and *Ptgdr2* (Fw TCCGCTACATCGACCACGTG, Rev GGATGAGTCCGTTTTCCACCA).

Immune and Angiogenic Profiling

1×10^6 IL-4–polarized macrophages (Ctrl or $Hpgds^{\Delta M\phi}$) were seeded in 24-well plates in DMEM supplemented with 10% FBS, 1% penicillin/streptomycin, and 1% L-Glut. Two days after polarization, macrophages were collected in RLT buffer, and RNA from cells was extracted following the protocol described above. The primers used to assess gene expression are listed in the section "Primers/Probes". The data are visualized as a heatmap using the "pheatmap" package in the R program.

Flow Cytometry

Cells were counted and blocked by using BD Fc Block Purified Rat Anti-Mouse CD16/CD32 mAb (BD Pharmingen, 553142, RRID: AB_394657). For extracellular staining, cells were stained for 30 minutes on ice with the following antibodies: fixable viability dye (eF450, eBioscience, 65-0863-18; eF506, eBioscience, 65-0866-14; or eF780, Thermo Fisher Scientific, 65-0865-18), anti-CD45 (BioLegend, 103112, RRID: AB_312977; BioLegend, 103132, RRID: AB_893340; BioLegend, 103116, RRID: AB_312981; BD Biosciences, 564279, RRID: AB_2651134; BD Biosciences, 748371, RRID: AB_2872790), anti-CD11b (BD Biosciences, 749864, RRID: AB_2874105; BD Biosciences, 741934, RRID: AB_2871246; BD Biosciences, 557397, RRID: AB_396680; eBioscience, 25-0112-81, RRID: AB_469587), anti-F4/80 (eBioscience, 17-4801-82, RRID: AB_2784648; eBioscience, 48-4801-82, RRID: AB_1548747; eBioscience, 53-4801-82, RRID: AB_469915; Thermo Fisher Scientific, 404-4801-80, RRID: AB_2925526; BioLegend, 123133, RRID: AB_2562305), anti–MHC-II (eBioscience, 17-5321-81, RRID: AB_469454; BioLegend, 107627, RRID: AB_1659252), anti-CD80 (BioLegend, 104743, RRID: AB_2810338), anti-CD86 (BioLegend, 105007, RRID: AB_313150), anti-CD11c (Thermo Fisher Scientific, 17-01114-82, RRID: AB_469346; eBioscience, 25-0114-82, AB_469590), anti-CD206 (Thermo Fisher Scientific, 17-2061-82, RRID: AB_2637420; BD Biosciences, 568817, RRID: AB_3073651), anti-CD204 (Miltenyi Biotec, 130-102-251, RRID: AB_2656169), anti-CD8a (BD Biosciences, 553035, RRID: AB_398527; BD Biosciences, 612898, RRID: AB_2870186; BioLegend, 100713, RRID: 312752), and anti-CD69 (BioLegend, 104522, RRID: 2260065). Afterward, cells were washed in FACS buffer (PBS containing 2% FBS and 2 mmol/L EDTA) and fixed in a 1:1 mixture of IC fixation buffer (eBioscience, 00-8222-49) and FACS buffer and analyzed using a BD Fortessa X-20 (BD Biosciences). For the intracellular measurements of TNFα (BioLegend, 506346, RRID: AB_2565955), IFNγ (Thermo Fisher Scientific, 25-7311-82, 469680; BioLegend, 505808, RRID: AB_315401), and GZMB (BioLegend, 515406, RRID: AB_2566459), single-cell suspensions were stimulated with phorbol 12-myristate 13-acetate/ionomycin cell stimulation cocktail (eBioscience, 00-4970-03) in presence of brefeldin A (BioLegend, 420601) and monensin (eBioscience, 00-4505-51) for 4 hours at 37°C in RPMI supplemented with 10% FBS and 1% penicillin/streptomycin. Afterward, cells were stained for surface markers, followed by 30 minutes incubation in Fix/Perm (Invitrogen, 00-5523-00) at 4°C. Cells were then washed with permeabilization buffer and stained overnight with the following antibodies: anti-TNFα, anti-IFNγ, and anti-GZMB. Cells were subsequently washed, resuspended in cold FACS buffer, and analyzed using a BD Fortessa X-20 (BD Biosciences). For the human staining, cells were counted and blocked using an anti-human Fc Receptor Binding Inhibitor (eBioscience, 14-9161-73, RRID: AB_468582). Cells were then stained by using the following antibodies: anti-CD80 (BD Biosciences, 557227, RRID: AB_396606), anti–HLA-DR (Thermo Fisher, 17-9956-42, RRID: AB_10670347), anti-CD163 (Sony Biotech, 2268080), and anti-CD206 (BD Biosciences, 740309, RRID: AB_2740047). FACS data were acquired by FACS Fortessa (BD Biosciences). Fluorescence minus one controls and an unstained control were used to ensure proper gating of positive populations. Data were analyzed by using FlowJo software (TreeStar v10.9.0).

Cell Sorting

1×10^6 YUMM1.7 CD90.1$^+$ cells were intradermally injected in the right flank of the mouse. Tumors were harvested for FACS as previously mentioned. After obtaining a single-cell suspension, CD45 enrichment was done by following the manufacturer's instructions (CD45 MicroBeads, Miltenyi Biotech, 130-052-301). Cells (CD45$^+$ and CD45$^-$) were then incubated with Mouse BD Fc Block Purified Rat Anti-Mouse CD16/CD32 mAb (BD Pharmingen, 553142, RRID: AB_394657) for 15 minutes at 4°C and stained with the following antibodies for 30 minutes at 4°C: fixable viability dye (eF450, eBioscience, 65-0863-18 or eF506, eBioscience 65-0866-14), anti-CD45 (BioLegend, 103112, RRID: AB_312977; BioLegend, 103132, RRID: AB_893340; BioLegend, 103,116, RRID: AB_312981; BD Biosciences, 564279, RRID: AB_2651134; BD Biosciences, 748371, RRID: AB_2872790), anti-CD11b (BD Biosciences, 749864, RRID: AB_2874105; BD Biosciences, 741934, RRID: AB_2871246; BD Biosciences, 557397, RRID: AB_396680; eBioscience, 25-0112-81, RRID: AB_469587), anti-F4/80 (eBioscience, 17-4801-82, RRID: AB_2784648; eBioscience, 48-4801-82, RRID: AB_1548747; eBioscience, 53-4801-82, RRID: AB_469915; Thermo Fisher Scientific, 404-4801-80, RRID: AB_2925526; BioLegend, 123133, RRID: AB_2562305), anti-Tcrβ chain (BD Biosciences, 562839, RRID: AB_2737830), anti-CD8a (BD Biosciences, 553035, RRID: AB_398527; BD Biosciences, 612898, RRID: AB_2870186; BioLegend, 100713, RRID: 312752), anti-CD4 (BioLegend, 100540, RRID: AB_893332), anti-CD370 (BioLegend, 143506, RRID: AB_2566380), anti-CD90.1 (BD Biosciences, 202506, RRID: AB_492882), anti-CD90.2 (BD Biosciences, 553005, RRID: AB_394544), anti-CD31 (BD Biosciences, 551262, RRID: AB_398497), anti-Ly6G (BioLegend, 127624, RRID: AB_10640819; BD Biosciences, 551461, RRID: AB_394208), anti-CD115 (BioLegend, 135523, RRID: AB_2566459), anti-FcεR1α (BD Biosciences, 751766, RRID: AB_2875743), anti-CD117 (BioLegend, 105828, RRID: AB_11204256), anti–MHC-II (eBioscience, 17-5321-81, RRID: AB_469454; BioLegend, 107627, RRID: AB_1659252), anti-CD11c (Thermo Fisher Scientific, 17-01114-82, RRID: AB_469346; eBioscience, 25-0114-82, AB_469590), anti-CD279/PD1 (BioLegend, 135217, RRID: AB_10900085; BioLegend, 135208, RRID: AB_2159184), and anti-CXCR5 (BD Biosciences, 563981, RRID: AB_2738522). Cells were washed, resuspended in cold FACS buffer (PBS containing 2% FBS and 2 mmol/L EDTA), and sorted using a FACSAria III (BD Biosciences) flow cytometer. Fluorescence minus one and unstained controls were used to ensure proper gating of positive populations.

Lipid Extraction

The extraction protocol was adapted from an already-described method (81). Tissue samples were mixed with methanol containing 100 picograms deuterated internal standards and 10 µL antioxidant mix [100 µmol/L indomethacin, 0.2 mg/mL BHT, and 100 µmol/L trans-4-(-4-(3-adamantan-1-yl-ureido9-cyclohexyloxy)-benzoic acid in MeOH] and were homogenized using a Precellys system at 4°C. The homogenized samples were stored at −80°C for 30 minutes and then centrifuged at 16,000 *g* for 10 minutes at 4°C. The supernatant was transferred to a new tube and diluted with water to achieve a methanol percentage <10%. The remaining pellet was redissolved in TE buffer for DNA concentration determination (Hoechst assay). Lipids were extracted using Strata-X 33 µm Polymeric Reversed Phase extraction columns (Phenomenex, 8B-S100-ECH) as instructed by the manufacturer. Briefly, the columns were preconditioned with 3 mL methanol, followed by 3 mL water. The sample (containing <10% methanol) was eluted dropwise, followed by a wash step with 3 mL of 10% methanol and elution with 100% methanol into a glass collection tube containing 6 µL of a 30% glycerol in methanol solution. Samples were evaporated in a vacuum centrifuge, redissolved in a 1:1 solution of water/methanol, and transferred to an LC vial.

LC-MS/MS

Lipid species were analyzed by LC/MS-MS on a Nexera X2 UHPLC system (Shimadzu) coupled with a hybrid triple-quadrupole/linear ion trap mass spectrometer (QTRAP 6500+ system; SCIEX). Chromatographic separation was performed on a Polar C18 column (2.6 µm, 3.0 × 100 mm; Phenomenex) maintained at 50°C using mobile phase A (0.1% formic acid in water) and mobile phase B (0.1% formic acid in methanol) in the following gradient: (0–2 minutes: 45% B; 2–16.5 minutes: 45% B → 80% B; 16.5–18.5 minutes: 98% B; and 18.5–20.5 minutes: 10% B) at a flow rate of 0.5 mL/minutes. The instrument parameters were as follows: curtain gas = 30 psi; collision gas = eight a.u. (medium); IonSpray voltage = 5,200 V and −4,200 V; temperature = 520°C; ion source gas 1 = 50 psi; and ion source gas 2 = 70 psi. The endocannabinoids, LTC4, LTD4, LTD4, 2-AG, MTCR, and PTCR compounds were detected in positive ion mode, and all other compounds were detected in negative ion mode. Multiple Reaction Monitoring (MRM) transitions were sourced from (82, 83).

Histology and Immunostainings

Murine tumors were collected and fixed in 4% paraformaldehyde (PFA) overnight at 4°C, dehydrated, and embedded in paraffin. Serial sections of 7-µm thickness were cut using a Microm HM360 Microtome. Human melanoma samples were obtained as 7-µm-thick paraffin-embedded slides. Paraffin slides were rehydrated to further proceed with antigen retrieval solution (Agilent, S1699) for 20 minutes at 100°C. After 20 minutes of cooling down, the sections were washed with TBS and kept in methanol. If necessary, 0.3% H_2O_2 was added to methanol to inactivate endogenous peroxidases. The samples were washed and blocked with the appropriate serum (preimmune donkey serum D9663 or preimmune goat serum G9023, Sigma-Aldrich) diluted 1:5 in Tris–NaCl-blocking buffer (TNB). Subsequently, the sections were incubated overnight with the following antibodies: rat anti-HPGDS (Cayman Chemical Company, 10004349, RRID: AB_327816; Cayman Chemical Company, 10004348, RRID: AB_10079369), rabbit anti-F4/80 (Cell Signaling Technology, 70076, RRID: AB_2799771), rat anti-F4/80 (Bio-Rad, MCA497G, RRID: AB_872005), goat anti-MMR/CD206 (R&D Systems, AF2535, RRID: AB_2063012), rabbit anti-CD80 (Abcam, ab64116, RRID: AB_1640342), rabbit anti-CD8 (Cell Signaling Technology, 98941S, RRID: AB_2756376), rat anti-mouse Ly6G (BD Biosciences, 551459, RRID: AB_394206), rat anti-CD4 (Thermo Fisher Scientific, 14-9766-95, RRID: AB_2865432), goat anti-CD105/Endoglin (R&D Systems, AF1320, RRID: AB_354735), rabbit anti–αSMA-Cy3 (Sigma-Aldrich, C6198, RRID: AB_476856), rabbit anti-hypoxyprobe (Hypoxyprobe Kit, Chemicon, PAb2627), rabbit anti-FITC (Bio-Rad, 4510-7604, RRID: AB_620673), anti-human CD163 (Leica Biosystems, NCL-L-CD163, RRID: AB_2756375), anti-human HPGDS (R&D Systems, MAB6487, RRID: AB_10972458), and anti-human CD8 (Agilent, GA623, RRID: AB_3073940). Murine lungs were collected and fixed in 2% PFA overnight at 4°C, dehydrated, and embedded in paraffin. Serial sections of 7 µm thickness were cut using a Microm HM360 Microtome. Paraffin slides were rehydrated to further proceed with antigen retrieval solution (Agilent, S1699) for 40 minutes at 100°C. After 40 minutes of cooling down, the sections were washed with TBS and kept for 20 minutes in methanol with 0.3% H_2O_2 to inactivate endogenous peroxidases. Samples were washed and blocked for 30 minutes with preimmune goat serum (Sigma-Aldrich, G9023) diluted 1:5 in TNB and 1 hour with purified rat anti-mouse (BD Biosciences, 553142; RRID: AB_394657) diluted 1:5 in TNB. Afterward, the sections were incubated overnight with anti-mouse CD90.1 (Thermo Fisher Scientific, 14-0900-81, RRID: AB_467373). Next, Hoechst 33342 (Thermo Fisher Scientific, H3570) together with appropriate antibodies were applied, including Alexa 488, 568, or 647 conjugated secondary antibodies (Invitrogen) or biotin-labeled antibodies (Jackson Immunoresearch). After biotin-labeled antibodies, TSA cyanine 3 (PerkinElmer, Life Sciences, NEl704A001KT), TSA cyanine 5 (PerkinElmer, Life Sciences, NEL705001KT), or TSA fluorescein (PerkinElmer, Life Sciences, NEL701001KT) system amplification kits were used according to the manufacturer's instructions. The sections were then mounted with ProLong Gold mounting medium without DAPI (4′,6-Diamidino-2-phenylindole dihydrochloride, Thermo Fisher Scientific, P36930). Imaging and microscopic analyses were performed with an Olympus BX41 microscope and CellSense imaging software.

Hypoxia Assessment and Tumor Perfusion

For the detection of tumor hypoxia, tumors were collected 1h after intraperitoneal injection of 60 mg/kg pimonidazole hydrochloride Hypoxyprobe-1 Omni Kit, (Hypoxyprobe cat. # HP3-100 Kit, RRID: AB_2934099) into melanoma-bearing mice. To detect the formation of pimonidazole adducts, 7-µm sections were stained with rabbit anti-hypoxyprobe mAb following the manufacturer's instructions. To analyze vessel perfusion, tumors were collected 15 minutes after retro-orbital injection of 0.05 mg of FITC-conjugated lectin (*Lycopersicon esculentum*; Vector Laboratories, B-1175-1).

PDOTSs

The clinical protocol was approved by the Ethical Committee of the University Hospitals Gasthuisberg KU Leuven (S67821) after obtaining written informed consent. Human melanoma sample was received in cold RPMI (Gibco, 21,875-034) complete supplemented with 10% FBS (Biowest, S00F9110002), 1% penicillin/streptomycin (Gibco, 15140-122) on ice and minced in 13.5 mL RPMI supplemented with 10% FBS, 0.5% penicillin/streptomycin, 1.1 mg/mL collagenase I (Thermo Fisher Scientific, 17100017), 2.3 mg/mL Dispase II (Thermo Fisher Scientific, 17105041), and 2.2 µL DNase I (Sigma-Aldrich, 11284932001) and digested for 20 minutes at 37°C. Digested tissue was centrifuged for 5 minutes at 1,500 rpm, resuspended in RPMI complete, and filtered using first a 100-µm and then a 40-µm mesh strainer to generate S2 fraction (40–100 µm) spheroid fractions. This fraction was then centrifuged at 1,500 rpm for 5 minutes at 4°C and resuspended in a matrix, containing 2.5 mg/mL type I rat tail collagen (Sigma-Aldrich, 08-115) buffered with PBS 10× with phenol red and with the pH adjusted to 7.4 using 0.5 mol/L NaOH. The mixture containing the spheroid embedded in the collagen was then loaded into the 3D microfluidic culture devices (AimBiotech).

Spheroids were then incubated for 40 minutes at 37°C to let the collagen solidify and then hydrated with DMEM supplemented with 10% FBS and 10% penicillin/streptomycin. After 24 hours, PDOTSs were treated with 1 μmol/L HQL-79 or with vehicle by refreshing the inhibitor every day for an additional 96 hours. After 24 hours of culture, PDOTSs were stained for confocal imaging. Briefly, the medium was washed out with PBS, and an anti-human Fc receptor binding inhibitor (eBioscience, 14-9161-73; RRID: AB_468582) was added to the PDOTSs. After 30 minutes of incubation, blocking was washed out with PBS, and a staining mix containing the following antibodies was added for 60 minutes at RT: calcein-AM (Sigma-Aldrich, 206700, RRID: AB_3665438) and anti-CD8 AF555 (Thermo Fisher Scientific, BS-0648R-A555, RRID: AB_3665439) or anti-CD68 AF594 (Biotechne, IC20401T-100UG) and CD163 (Leica Biosystems, NCL-L-CD163, RRID: AB_2756375). Primary antibodies were washed out, and PDOTSs were incubated for another 60 minutes at RT with an anti-rabbit AF647 antibody (Thermo Fisher Scientific, A-31573). After the staining, channels were rehydrated with RPMI without phenol red supplemented with 10% FBS, 1% penicillin/streptomycin, and 1% L-Glut. PDOTSs were imaged once per day for three consecutive days on a Nikon TiE A1R microscope using a 20× objective in Galvano mode. Image analysis was done using the NIS-Elements software. After 96 hours treatment, PDOTSs were then digested by incubating the spheroids with digestion medium for 15 minutes at 37°C, collected, and transferred into the FACS tubes. Cells were then incubated with Fc Receptor Binding Inhibitor Polyclonal Antibody (Thermo Fisher Scientific, 14-9161-73, RRID: AB_468582) for 15 minutes at 4°C and stained with the following antibodies for 30 minutes at 4°C: fixable viability dye (eF450), anti-CD45 (Sony Biotechnology, 2120250, RRID: AB_3665367), anti-CD8a (BioLegend 301012, RRID: AB_314130), anti–HLA-DR (Thermo Fisher, 17-9956-42; RRID: AB_10670347), anti-CD11b (BioLegend, 101227, RRID: AB_893233), anti-CD68 (R&D Systems, IC20401T, RRID: AB_3654930), and anti-TNFα (BioLegend, 986,802, RRID: AB_2941660). FACS data were acquired by FACS Fortessa (BD Biosciences). Data were analyzed by using FlowJo (TreeStar).

Bioinformatics

For the in-house scRNA-seq data from immune cells was acquired from the Landeloos and colleagues study (bioRxiv 2023.12.14.571631). Briefly, the study included treatment-naïve stage III/IV (AJCC 8th edition) patients with melanoma receiving αPD1-based therapy [αPD1 monotherapy (nivolumab): $n = 17$; αPD1 and αCTLA4 combination therapy (ipilimumab + nivolumab): ($n = 6$) SPECIAL trial; UZ/KU Leuven #S62275]. Cutaneous, subcutaneous, or lymph node metastases were biopsied before initiation of therapy. Subsequently, a second tumor biopsy was collected right before the administration of the second ICB treatment cycle (early OT). Response of the patients to the treatment was stratified based on RECIST v1.1. Immune cells were identified based on unsupervised clustering and DEGs per cluster. Further details about data processing are described in Landeloos and colleagues study (bioRxiv 2023.12.14.571631). Analysis corresponding to the different macrophage subpopulations, YUMM1.7, and patients was done using R v.4.2.3 and the Seurat package (v4.3.0). An initial exploratory analysis was conducted to investigate the changes between the macrophages in Rs and NRs. Specifically, the LYVE1 macrophages showed an overlap between their DEGs and genes associated with the arachidonic acid metabolism pathway retrieved from the Kyoto Encyclopedia of Genes and Genomes database (https://www.kegg.jp/entry/hsa00590). The list of DEGs was selected based on the FindAllMarkers function using $\log_2$ fold change >1.5 and an adjusted P value < 0.05. The scRNA-seq data for the YUMM1.7 tumor model and patients with melanoma were sourced from three Gene Expression Omnibus (RRID: SCR_005012) datasets with the following accession numbers: GSE146613, GSE115978, and GSE120575. Cells were filtered out if they had fewer than 200 or more than 6,000 detected genes or if mitochondrial transcripts constituted more than 10% of the reads. Similarly, genes were excluded if they were detected in fewer than three cells. Scaling, normalization, and clustering were done using the default Seurat pipeline and options for this version. Uniform Manifold Approximation and Projections were generated for visualization of the data. Differential gene expression analysis between each cluster was performed using a Wilcoxon rank-sum test. In the murine scRNA-seq dataset, previously reported marker genes were used to annotate different macrophage subpopulations, including *Ifn*$^+$ macrophages (*C1qa*, *Cd80*, *Cd86*, *Itgax*, *Tlr2, Fcgr1*, *Il1b*, *Ifngr1*, and *Ifngr2*) and *Mrc1*$^+$ macrophages (*C1qa*, *Mrc1*, *Sepp1*, *Ctsb*, *Retnla*, and *Cd200r1*). The R package ggplot2 v3.4.1 was used to check HPGDS expression in different clusters of cells. Cutoff thresholds, distinguishing high and low HPGDS expression, were determined by evaluating the expression patterns in violin plots. Macrophages were selected if they expressed HPGDS and divided into HPGDS^{High} and HPGDS^{Low} groups for subsequent differential analysis. The percentage of HPGDS$^+$ macrophages was calculated as a fraction of all macrophages for each patient. The statistical test to compare groups was the Wilcoxon rank-sum test.

RNA-seq on

Total RNA was isolated from *in vivo* sorted *Hpgds* KO and Ctrl TAMs (viability$^-$, CD45$^+$, CD11b$^+$, F4/80$^+$) using RNeasy Minikit (Qiagen, 74106) following the manufacturer's protocol and resuspended in RNase-free water. Frozen RNA samples were shipped to Novogene for the Plant and Animal Eukaryotic Strand Specific mRNA (WOBI) service, and the resulting paired-end 150bp reads were sequenced on a Novaseq X Plus instrument (RRID: SCR_024568). Next, reads were aligned to the *Mus musculus* reference genome GRCm39 using STAR (v2.7.10b; RRID: SCR_004463) with default parameters, resulting in an average of 33.6 million uniquely mapped reads per sample. Aligned reads were quantified using featureCounts (v2.0.1; RRID: SCR_012919) in R (v4.3.3; RRID: SCR_001905) with options -t gene and -s 2. Subsequent analyses were performed with DESeq2 package (v1.42.0; RRID: SCR_015687; ref. 84). Gene Set Enrichment Analysis was conducted with clusterProfiler (v4.10.0; RRID: SCR_016884) and org.Mm.eg.db (v3.18.0; RRID: SCR_023488) and visualized using DOSE (v3.28.1) and enrichplot (v1.22.0; refs. 85, 86). Marker genes of Immunosuppressive TAMs were defined above (as Mrc1-immunosuppressive macrophages). The angiogenesis-related cytokines signature includes *Fgf2*, *Pdgfc*, *Egf*, *Hgf*, *Pdgfa*, *Tgfa*, *Angpt2*, *Vegfc*, *Angpt1*, *Pdgfb*, *Vegfa*, *Vegfb*, *Igf1*, and *Pigf*.

Analysis of TCGA Data

Gene expression and clinical data for TCGA SKCM were obtained from cBioPortal (https://www.cbioportal.org/datasets). The gene expression values were normalized to transcripts per million for subsequent analysis. The infiltration of 22 types of immune cells in each melanoma sample was determined using the CIBERSORT package (v0.1.0) in R software. Gene set permutations were set at 1,000 repeats for each analysis. The R package ggpubr (v0.6.0) was used to elucidate the differences between TME scores and *HPGDS* levels in these patients. To investigate the expression of *HPGDS* in human PDAC, normalized RNA-seq expression data from 177 PDAC tissue samples and 167 normal pancreatic samples were obtained from cBioPortal and the Genome–Tissue Expression project (https://www.genome.gov/Funded-Programs-Projects/Genotype-Tissue-Expression-Project), respectively. *HPGDS* expression levels were compared between tumor and normal tissues using the TCGA and Genome–Tissue Expression datasets. The Limma package was used to adjust batch effects between the two datasets. Gene expression distributions are presented as box plots, with statistical significance calculated using the Wilcoxon test.

Statistics

Data entry was performed in a blind fashion. All statistical analyses were performed using GraphPad Prism software (version 10.0.2). Statistical significance was calculated by two-tailed unpaired Student *t* tests on two experimental conditions and one-way or two-way ANOVA when repeated measures were compared. All the results are shown as the mean ± SEM. Statistics were indicated only when significant. Detection of mathematical outliers was performed using the Grubb test in GraphPad. Sample sizes for all experiments were selected based on those reported in previous studies. Animals were excluded if they died or had to be killed according to protocols approved by the animal experimental committees.

Data Availability

The software used in this study are all published and cited in the main text or "Methods". The source code is available on GitHub (https://github.com/mazzonelab/HPGDS_CancerDiscovery2024) and Code Ocean (https://codeocean.com/capsule/0921751). The bulk RNA-seq data generated in this study are publicly available in Gene Expression Omnibus GSE281745.

Authors' Disclosures

R. Trotta reports a patent for EP23210278.0 pending, a patent for EP23210284.8 pending, and a patent for EP23210290.5 pending. S. Rivis reports other support from Kom op tegen Kanker (STK) and Fonds Wetenschappelijk Onderzoek (FWO; 1197720N, 1197722N) outside the submitted work. S. Zhao reports grants from the Chinese Scholarship Council outside the submitted work. M.-P. Orban reports other support from Fonds voor wetenschappelijk onderzoek (1124423N and 1124425N) and Kom op tegen kanker- Evds grant outside the submitted work. I. Charatsidou reports other support from FWO (1SH4S24N) outside the submitted work. F.M. Bosisio reports grants from FWO during the conduct of the study. M. Mazzone reports grants from ERC Consolidator, ERC Proof-of-Concept, the Belgian Foundation against Cancer, FWO research grant, and FWO Strategic Basic Research during the conduct of the study, as well as other support from iTeos Therapeutics and personal fees and other support from Montis Biosciences outside the submitted work; in addition, M. Mazzone has a patent for EP23210278.0 pending, a patent for EP23210284.8 pending, and a patent for EP23210290.5 pending. No disclosures were reported by the other authors.

Authors' Contributions

R. Trotta: Conceptualization, funding acquisition, validation, writing–original draft, writing–review & editing. **S. Rivis:** Validation. **S. Zhao:** Data curation, validation. **M.-P. Orban:** Validation. **S. Trusso Cafarello:** Validation. **I. Charatsidou:** Validation. **J. Pozniak:** Data curation. **J. Dehairs:** Data curation. **L. Vanheer:** Data curation. **C.A. Pulido Vicuna:** Data curation. **V. Boecxstaens:** Resources. **O. Bechter:** Resources. **F.M. Bosisio:** Resources. **J.V. Swinnen:** Resources. **J.-C. Marine:** Resources. **M. Mazzone:** Conceptualization, supervision, funding acquisition, writing–original draft, writing–review & editing.

Acknowledgments

M. Mazzone was supported by the European Research Council Consolidator grant (ImmunoFit, 773208), the Belgian Foundation against Cancer – Stichting tegen Kanker (F/2020/1372), and Fonds Wetenschappelijk Onderzoek (FWO; G082323N). The project received support from the European Research Council (European Research Council PoC; EicoMet, 101123280). M. Mazzone and J.V. Swinnen were supported by FWO – Strategic Basic Research grant (LipoMacs, S001623N). J. Pozniak received financial support from the Marie Curie Individual Fellowship (H2020-MSCA-IF-2019, 896897). I. Charatsidou was funded by FWO (1SH4S24N). M.-P. Orban was funded by Kom op tegen Kanker (STK) and FWO (1124423N). S. Zhao was funded by the China Scholarship Council (202106940001). S. Rivis was funded by Kom op tegen Kanker (STK) and FWO (1197720N and 1197722N). We thank the VIB FACS Expertise Centre Leuven for the flow cytometry measurements. We thank the Wellcome Trust Sanger Institute Mouse Genetics Project and its funders for providing the mutant mouse line C57BL/6NTac-Fcγr1$^{tm(EGFP/Cre/ERT2)Wtsi}$/WtsiH and the European Mouse Mutant Archive (www.infrafrontier.eu; Repository number EM: 11125) partner at the Mary Lyon Centre at MRC Harwell from which the mouse line was received. This work is dedicated to the late G. Argentieri. We also thank M. Di Matteo for help in gene editing, A. Talebi for advice, F. Seminara, G. Volpato, G. Maspero, and N. Marchetti for technical support.

Note

Supplementary data for this article are available at Cancer Discovery Online (http://cancerdiscovery.aacrjournals.org/).

Received March 22, 2024; revised November 22, 2024; accepted March 13, 2025; posted first April 7, 2025.

REFERENCES

1. Waldman AD, Fritz JM, Lenardo MJ. A guide to cancer immunotherapy: from T cell basic science to clinical practice. Nat Rev Immunol 2020;20:651–68.
2. Long GV, Swetter SM, Menzies AM, Gershenwald JE, Scolyer RA. Cutaneous melanoma. Lancet 2023;402:485–502.
3. Huang AC, Zappasodi R. A decade of checkpoint blockade immunotherapy in melanoma: understanding the molecular basis for immune sensitivity and resistance. Nat Immunol 2022;23:660–70.
4. Rauwerdink DJW, Molina G, Frederick DT, Sharova T, Van Der Hage J, Cohen S, et al. Mixed response to immunotherapy in patients with metastatic melanoma. Ann Surg Oncol 2020;27:3488–97.
5. Arnold M, Singh D, Laversanne M, Vignat J, Vaccarella S, Meheus F, et al. Global burden of cutaneous melanoma in 2020 and projections to 2040. JAMA Dermatol 2022;158:495–503.
6. Khan SU, Khan MU, Azhar Ud Din M, Khan IM, Khan MI, Bungau S, et al. Reprogramming tumor-associated macrophages as a unique approach to target tumor immunotherapy. Front Immunol 2023;14:1166487.
7. Mantovani A, Marchesi F, Malesci A, Laghi L, Allavena P. Tumour-associated macrophages as treatment targets in oncology. Nat Rev Clin Oncol 2017;14:399–416.
8. Luo X, Zhao X, Cheng C, Li N, Liu Y, Cao Y. The implications of signaling lipids in cancer metastasis. Exp Mol Med 2018;50:1–10.
9. Morotti M, Grimm AJ, Hope HC, Arnaud M, Desbuisson M, Rayroux N, et al. PGE_2 inhibits TIL expansion by disrupting IL-2 signalling and mitochondrial function. Nature 2024;629:426–34.
10. Lacher SB, Dörr J, De Almeida GP, Hönninger J, Bayerl F, Hirschberger A, et al. PGE_2 limits effector expansion of tumour-infiltrating stem-like $CD8^+$ T cells. Nature 2024;629:417–25.
11. Elewaut A, Estivill G, Bayerl F, Castillon L, Novatchkova M, Pottendorfer E, et al. Cancer cells impair monocyte-mediated T cell stimulation to evade immunity. Nature 2025;637:716–25.
12. Böttcher JP, Bonavita E, Chakravarty P, Blees H, Cabeza-Cabrerizo M, Sammicheli S, et al. NK cells stimulate recruitment of cDC1 into the tumor microenvironment promoting cancer immune control. Cell 2018;172:1022–37.e14.
13. Zelenay S, van der Veen AG, Böttcher JP, Snelgrove KJ, Rogers N, Acton SE, et al. Cyclooxygenase-Dependent tumor growth through evasion of immunity. Cell 2015;162:1257–70.

14. Wang T, Jing B, Xu D, Liao Y, Song H, Sun B, et al. PTGES/PGE_2 signaling links immunosuppression and lung metastasis in Gprc5a-knockout mouse model. Oncogene 2020;39:3179–94.
15. Markosyan N, Li J, Sun YH, Richman LP, Lin JH, Yan F, et al. Tumor cell-intrinsic EPHA2 suppresses anti-tumor immunity by regulating PTGS2 (COX-2). J Clin Invest 2019;129:3594–609.
16. Johnson AM, Kleczko EK, Nemenoff RA. Eicosanoids in cancer: new roles in immunoregulation. Front Pharmacol 2020;11:595498.
17. Wang D, DuBois RN. Role of prostanoids in gastrointestinal cancer. J Clin Invest 2018;128:2732–42.
18. Tokudome S, Sano M, Shinmura K, Matsuhashi T, Morizane S, Moriyama H, et al. Glucocorticoid protects rodent hearts from ischemia/reperfusion injury by activating lipocalin-type prostaglandin D synthase–derived PGD2 biosynthesis. J Clin Invest 2009;119:1477–88.
19. Jowsey IR, Thomson AM, Flanagan JU, Murdock PR, Moore GB, Meyer DJ, et al. Mammalian class Sigma glutathione S-transferases: catalytic properties and tissue-specific expression of human and rat GSH-dependent prostaglandin D2 synthases. Biochem J 2001;359:507–16.
20. Murata T, Aritake K, Matsumoto S, Kamauchi S, Nakagawa T, Hori M, et al. Prostagladin D2 is a mast cell-derived antiangiogenic factor in lung carcinoma. Proc Natl Acad Sci U S A 2011;108:19802–7.
21. Omori K, Morikawa T, Kunita A, Nakamura T, Aritake K, Urade Y, et al. Lipocalin-type prostaglandin D synthase-derived PGD_2 attenuates malignant properties of tumor endothelial cells: L-PGDS-derived PGD_2 moderates tumor endothelial cell behavior. J Pathol 2018;244:84–96.
22. Jerby-Arnon L, Shah P, Cuoco MS, Rodman C, Su M-J, Melms JC, et al. A cancer cell program promotes T cell exclusion and resistance to checkpoint blockade. Cell 2018;175:984–97.e24.
23. Sade-Feldman M, Yizhak K, Bjorgaard SL, Ray JP, De Boer CG, Jenkins RW, et al. Defining T cell states associated with response to checkpoint immunotherapy in melanoma. Cell 2018;175:998–1013.e20.
24. Bill R, Wirapati P, Messemaker M, Roh W, Zitti B, Duval F, et al. CXCL9:SPP1 macrophage polarity identifies a network of cellular programs that control human cancers. Science 2023;381:515–24.
25. Piras F, Colombari R, Minerba L, Murtas D, Floris C, Maxia C, et al. The predictive value of CD8, CD4, CD68, and human leukocyte antigen-D-related cells in the prognosis of cutaneous malignant melanoma with vertical growth phase. Cancer 2005;104:1246–54.
26. Ostendorf BN, Bilanovic J, Adaku N, Tafreshian KN, Tavora B, Vaughan RD, et al. Common germline variants of the human APOE gene modulate melanoma progression and survival. Nat Med 2020;26:1048–53.
27. Mary R, Chalmin F, Accogli T, Bruchard M, Hibos C, Melin J, et al. Hematopoietic prostaglandin D2 synthase controls tfh/Th2 communication and limits Tfh antitumor effects. Cancer Immunol Res 2022;10:900–16.
28. Wang J, Perry CJ, Meeth K, Thakral D, Damsky W, Micevic G, et al. UV -induced somatic mutations elicit a functional T cell response in the YUMMER 1.7 mouse melanoma model. Pigment Cell Melanoma Res 2017;30:428–35.
29. Jain RK. Normalization of tumor vasculature: an emerging concept in antiangiogenic therapy. Science 2005;307:58–62.
30. Jain RK. Normalizing tumor vasculature with anti-angiogenic therapy: a new paradigm for combination therapy. Nat Med 2001;7:987–9.
31. Rolny C, Mazzone M, Tugues S, Laoui D, Johansson I, Coulon C, et al. HRG inhibits tumor growth and metastasis by inducing macrophage polarization and vessel normalization through downregulation of PlGF. Cancer Cell 2011;19:31–44.
32. Huang Y, Snuderl M, Jain RK. Polarization of tumor-associated macrophages: a novel strategy for vascular normalization and antitumor immunity. Cancer Cell 2011;19:1–2.
33. Mazzone M, Dettori D, de Oliveira RL, Loges S, Schmidt T, Jonckx B, et al. Heterozygous deficiency of PHD2 restores tumor oxygenation and inhibits metastasis via endothelial normalization. Cell 2009;136:839–51.
34. Wenes M, Shang M, Di Matteo M, Goveia J, Martín-Pérez R, Serneels J, et al. Macrophage metabolism controls tumor blood vessel morphogenesis and metastasis. Cell Metab 2016;24:701–15.
35. Brown EB, Campbell RB, Tsuzuki Y, Xu L, Carmeliet P, Fukumura D, et al. In vivo measurement of gene expression, angiogenesis and physiological function in tumors using multiphoton laser scanning microscopy. Nat Med 2001;7:864–8.
36. Kong D, Shen Y, Liu G, Zuo S, Ji Y, Lu A, et al. PKA regulatory IIα subunit is essential for PGD2-mediated resolution of inflammation. J Exp Med 2016;213:2209–26.
37. Jandl K, Stacher E, Bálint Z, Sturm EM, Maric J, Peinhaupt M, et al. Activated prostaglandin D2 receptors on macrophages enhance neutrophil recruitment into the lung. J Allergy Clin Immunol 2016;137:833–43.
38. Aritake K, Kado Y, Inoue T, Miyano M, Urade Y. Structural and functional characterization of HQL-79, an orally selective inhibitor of human hematopoietic prostaglandin D synthase. J Biol Chem 2006;281:15277–86.
39. Cadilla R, Deaton DN, Do Y, Elkins PA, Ennulat D, Guss JH, et al. The exploration of aza-quinolines as hematopoietic prostaglandin D synthase (H-PGDS) inhibitors with low brain exposure. Bioorg Med Chem 2020;28:115791.
40. Aoyagi H, Kajiwara D, Tsunekuni K, Tanaka K, Miyoshi K, Hirasawa N. Potential synergistic effects of novel hematopoietic prostaglandin D synthase inhibitor TAS-205 and different types of anti-allergic medicine on nasal obstruction in a Guinea pig model of experimental allergic rhinitis. Eur J Pharmacol 2020;875:173030.
41. Dankort D, Curley DP, Cartlidge RA, Nelson B, Karnezis AN, Damsky WE Jr, et al. Braf(V600E) cooperates with Pten loss to induce metastatic melanoma. Nat Genet 2009;41:544–52.
42. Jenkins RW, Aref AR, Lizotte PH, Ivanova E, Stinson S, Zhou CW, et al. Ex vivo profiling of PD-1 blockade using organotypic tumor spheroids. Cancer Discov 2018;8:196–215.
43. Casazza A, Laoui D, Wenes M, Rizzolio S, Bassani N, Mambretti M, et al. Impeding macrophage entry into hypoxic tumor areas by Sema3A/nrp1 signaling blockade inhibits angiogenesis and restores antitumor immunity. Cancer Cell 2013;24:695–709.
44. Bieniasz-Krzywiec P, Martín-Pérez R, Ehling M, García-Caballero M, Pinioti S, Pretto S, et al. Podoplanin-expressing macrophages promote lymphangiogenesis and lymphoinvasion in breast cancer. Cell Metab 2019;30:917–36.e10.
45. Celus W, Di Conza G, Oliveira AI, Ehling M, Costa BM, Wenes M, et al. Loss of caveolin-1 in metastasis-associated macrophages drives lung metastatic growth through increased angiogenesis. Cell Rep 2017;21:2842–54.
46. Tu M, Klein L, Espinet E, Georgomanolis T, Wegwitz F, Li X, et al. TNF-α-producing macrophages determine subtype identity and prognosis via AP1 enhancer reprogramming in pancreatic cancer. Nat Cancer 2021;2:1185–203.
47. Nalio Ramos R, Missolo-Koussou Y, Gerber-Ferder Y, Bromley CP, Bugatti M, Núñez NG, et al. Tissue-resident $FOLR2^+$ macrophages associate with $CD8^+$ T cell infiltration in human breast cancer. Cell 2022;185:1189–207.e25.
48. Kiss M, Vande Walle L, Saavedra PHV, Lebegge E, Van Damme H, Murgaski A, et al. IL1β promotes immune suppression in the tumor microenvironment independent of the inflammasome and gasdermin D. Cancer Immunol Res 2021;9:309–23.
49. Diwakar BT, Yoast R, Nettleford S, Qian F, Lee T-J, Berry S, et al. Crth2 receptor signaling down-regulates lipopolysaccharide-induced NF-κB activation in murine macrophages via changes in intracellular calcium. FASEB J 2019;33:12838–52.
50. Dash P, Ghatak S, Topi G, Satapathy SR, Ek F, Hellman K, et al. High PGD2 receptor 2 levels are associated with poor prognosis in colorectal cancer patients and induce VEGF expression in colon cancer cells and migration in a zebrafish xenograft model. Br J Cancer 2022;126:586–97.
51. Gustafsson A, Hansson E, Kressner U, Nordgren S, Andersson M, Lönnroth C, et al. Prostanoid receptor expression in colorectal cancer related to tumor stage, differentiation and progression. Acta Oncol 2007;46:1107–12.
52. Fukuoka T, Yashiro M, Morisaki T, Kinoshita H, Hasegawa T, Kasashima H, et al. The role of type D prostanoid receptors and PPARγ in gastric cancer progression. Anticancer Res 2014;34:2771–8.

53. Quail DF, Joyce JA. Microenvironmental regulation of tumor progression and metastasis. Nat Med 2013;19:1423–37.
54. Andreu P, Johansson M, Affara NI, Pucci F, Tan T, Junankar S, et al. FcRgamma activation regulates inflammation-associated squamous carcinogenesis. Cancer Cell 2010;17:121–34.
55. Stockmann C, Doedens A, Weidemann A, Zhang N, Takeda N, Greenberg JI, et al. Deletion of vascular endothelial growth factor in myeloid cells accelerates tumorigenesis. Nature 2008;456:814–8.
56. Harney AS, Arwert EN, Entenberg D, Wang Y, Guo P, Qian B-Z, et al. Real-time imaging reveals local, transient vascular permeability, and tumor cell intravasation stimulated by TIE2hi macrophage-derived VEGFA. Cancer Discov 2015;5:932–43.
57. Wu VH, Yung BS, Faraji F, Saddawi-Konefka R, Wang Z, Wenzel AT, et al. The GPCR–$G\alpha_s$–PKA signaling axis promotes T cell dysfunction and cancer immunotherapy failure. Nat Immunol 2023;24:1318–30.
58. Kobayashi K, Omori K, Murata T. Role of prostaglandins in tumor microenvironment. Cancer Metastasis Rev 2018;37:347–54.
59. Ma R-Y, Black A, Qian B-Z. Macrophage diversity in cancer revisited in the era of single-cell omics. Trends Immunol 2022;43:546–63.
60. Guerriero JL, Sotayo A, Ponichtera HE, Castrillon JA, Pourzia AL, Schad S, et al. Class IIa HDAC inhibition reduces breast tumours and metastases through anti-tumour macrophages. Nature 2017;543:428–32.
61. Klug F, Prakash H, Huber PE, Seibel T, Bender N, Halama N, et al. Low-dose irradiation programs macrophage differentiation to an $iNOS^+$/M1 phenotype that orchestrates effective T cell immunotherapy. Cancer Cell 2013;24:589–602.
62. Horikami D, Sekihachi E, Omori K, Kobayashi Y, Kobayashi K, Nagata N, et al. Roles of lipocalin-type and hematopoietic prostaglandin D synthases in mouse retinal angiogenesis. J Lipid Res 2023;64:100439.
63. Finisguerra V, Di Conza G, Di Matteo M, Serneels J, Costa S, Thompson AAR, et al. MET is required for the recruitment of anti-tumoural neutrophils. Nature 2015;522:349–53.
64. Caronni N, La Terza F, Vittoria FM, Barbiera G, Mezzanzanica L, Cuzzola V, et al. IL-$1\beta^+$ macrophages fuel pathogenic inflammation in pancreatic cancer. Nature 2023;623:415–22.
65. Vandeusen CL, Weiberth FJ, Gill HS, Lee G, Hillegass A, inventor; Sanofi-aventis U.S. Inc., assignee. Phenyloxadialzole derivatives as PGDS inhibitors. France WO 2011044307. 2011 Apr 14.
66. Aldous SC, Fennie MW, Jiang JZ, John S, Mu L, Pedgrift B, inventor. et al; Sanofi-aventis U.S. Inc., assignee. Pyrimidine hydrazide compounds as PGDS inhibitors. France WO 2008121670. 2008 Oct 9.
67. Takeshita E, Komaki H, Shimizu-Motohashi Y, Ishiyama A, Sasaki M, Takeda S. A phase I study of TAS-205 in patients with Duchenne muscular dystrophy. Ann Clin Transl Neurol 2018;5:1338–49.
68. Cadilla R, Deaton DN, Hancock AP, Hobbs H, Hodgson ST, Larkin AL, inventor; et al. Astex Therapeutics Limited, GlaxoSmithKline Intellectual Property Development Limited, assignee. Quinoline-3-Carboxamides as h-pgds inhibitors. Great Britain WO 2017103851. 2017 Jun 22.
69. Hume DA, MacDonald KPA. Therapeutic applications of macrophage colony-stimulating factor-1 (CSF-1) and antagonists of CSF-1 receptor (CSF-1R) signaling. Blood 2012;119:1810–20.
70. MacDonald KPA, Palmer JS, Cronau S, Seppanen E, Olver S, Raffelt NC, et al. An antibody against the colony-stimulating factor 1 receptor depletes the resident subset of monocytes and tissue- and tumor-associated macrophages but does not inhibit inflammation. Blood 2010;116:3955–63.
71. Ahmad AS, Mendes M, Hernandez D, Doré S. Efficacy of laropiprant in minimizing brain injury following experimental intracerebral hemorrhage. Sci Rep 2017;7:9489.
72. Wong L-YR, Zheng J, Wilhelmsen K, Li K, Ortiz ME, Schnicker NJ, et al. Eicosanoid signalling blockade protects middle-aged mice from severe COVID-19. Nature 2022;605:146–51.
73. Takahashi G, Asanuma F, Suzuki N, Hattori M, Sakamoto S, Kugimiya A, et al. Effect of the potent and selective DP1 receptor antagonist, asapiprant (S-555739), in animal models of allergic rhinitis and allergic asthma. Eur J Pharmacol 2015;765:15–23.
74. Pellefigues C, Tchen J, Saji C, Lamri Y, Charles N. AMG853, A bispecific prostaglandin D_2 receptor 1 and 2 antagonist, dampens basophil activation and related lupus-like nephritis activity in lyn-deficient mice. Front Immunol 2022;13:824686.
75. Brightling CE, Gaga M, Inoue H, Li J, Maspero J, Wenzel S, et al. Effectiveness of fevipiprant in reducing exacerbations in patients with severe asthma (LUSTER-1 and LUSTER-2): two phase 3 randomised controlled trials. Lancet Respir Med 2021;9:43–56.
76. Philip G, Van Adelsberg J, Loeys T, Liu N, Wong P, Lai E, et al. Clinical studies of the DP1 antagonist laropiprant in asthma and allergic rhinitis. J Allergy Clin Immunol 2009;124:942–8.e1–9.
77. Bradley A, Anastassiadis K, Ayadi A, Battey JF, Bell C, Birling M-C, et al. The mammalian gene function resource: the international knockout mouse consortium. Mamm Genome 2012;23:580–6.
78. Schoors S, Bruning U, Missiaen R, Queiroz KCS, Borgers G, Elia I, et al. Fatty acid carbon is essential for dNTP synthesis in endothelial cells. Nature 2015;520:192–7.
79. Platt RJ, Chen S, Zhou Y, Yim MJ, Swiech L, Kempton HR, et al. CRISPR-Cas9 knockin mice for genome editing and cancer modeling. Cell 2014;159:440–55.
80. Qian B-Z, Li J, Zhang H, Kitamura T, Zhang J, Campion LR, et al. CCL2 recruits inflammatory monocytes to facilitate breast-tumour metastasis. Nature 2011;475:222–5.
81. Dumlao DS, Buczynski MW, Norris PC, Harkewicz R, Dennis EA. High-throughput lipidomic analysis of fatty acid derived eicosanoids and N-acylethanolamines. Biochim Biophys Acta 2011;1811:724–36.
82. Murphy RC. Tandem mass spectrometry of lipids. In: New developments in mass spectrometry; 2014. p. 280.[cited 2023 Aug 27]. Available from: https://books.rsc.org/books/book/1091/Tandem-Mass-Spectrometry-of-Lipids.
83. Stassburg K, Molloy BJ, Mallet C, Duesterloh A, Bendik I, Hankemeier T, et al. Targeted lipidomics of oxylipins (oxygenated fatty acids). 2015 [cited 2023 Aug 27]; Available from: http://rgdoi.net/10.13140/RG.2.1.3943.9207.
84. Love MI, Huber W, Anders S. Moderated estimation of fold change and dispersion for RNA-seq data with DESeq2. Genome Biol 2014;15:550.
85. Wu T, Hu E, Xu S, Chen M, Guo P, Dai Z, et al. clusterProfiler 4.0: a universal enrichment tool for interpreting omics data. Innovation (Camb) 2021;2:100141.
86. Yu G, Wang L-G, Yan G-R, He Q-Y. DOSE: an R/Bioconductor package for disease ontology semantic and enrichment analysis. Bioinformatics 2015;31:608–9.